FRONT MATTER

Title

Abrupt shift to El Niño-like mean state conditions in the tropical Pacific during the Little Ice Age

Authors

Ana Prohaska,[1,2,3*] Alistair W.R. Seddon,[4,5] Bernd Meese,[6] Katherine J. Willis,[1] John C. H. Chiang,[7,8] Dirk Sachse[9]

Affiliations

[1]Department of Zoology, University of Oxford, South Parks Road, Oxford OX1 3PS, UK.

[2]Department of Zoology, University of Cambridge, Downing St, Cambridge CB2 3EJ, UK.

[3]Lundbeck Foundation GeoGenetics Centre, GLOBE Institute, University of Copenhagen, Øster Voldgade 5-7, 1350 Copenhagen, Denmark (current affiliation).

[4]Department of Biology, University of Bergen, Post Box 7803, N-5020 Bergen, Norway.

[5]Bjerknes Centre for Climate Research, University of Bergen, Post Box 7803, N-5020 Bergen, Norway.

[6]Fraunhofer Institute for Manufacturing Engineering and Automation, Nobelstraße 12, 70569 Stuttgart, Germany.

[7]Department of Geography, University of California Berkeley, CA 94720-4740, USA.

[8] Berkeley Atmospheric Sciences Center, University of California Berkeley, CA 94720-4740, USA.

[9]GFZ-German Research, Centre for Geosciences, Section 4.6: Geomorphology, Organic Surface Geochemistry Lab, Telegrafenberg, Potsdam 14473, Germany.

*Corresponding author. Email: ana.prohaska@sund.ku.dk

This paper is a non-peer reviewed preprint submitted to EarthArXiv. This paper is in review at *Nature Geoscience*.

Abstract

The mean state of the tropical Pacific ocean-atmosphere climate, in particular its east-west asymmetry, has profound consequences for regional climates and for the El Niño/ Southern Oscillation variability. Here we present a new high-resolution paleohydrological record using the stable-hydrogen-isotopic composition of terrestrial-lipid biomarkers (δD_{wax}) from a 1,400-year-old lake sedimentary sequence from northern Philippines. Results show a dramatic and abrupt increase in δD_{wax} values around 1630 AD with sustained high values until 1900 AD. We interpret this change as a shift to sustained El Niño-like mean state conditions, and consequently, significantly drier conditions in the western tropical Pacific during the second half of the Little Ice Age. Our findings highlight the prominent role of the tropical Pacific in shaping the hydrology of the Tropics during the Little Ice Age and demonstrate that a marked transition in the tropical Pacific mean state can occur within a human lifetime.

37 **MAIN**

38 **Introduction**

39 A noticeable feature of the equatorial Pacific climate is its east-west asymmetry, with warmer
40 ocean surface conditions to the west that supports atmospheric deep convection, and a colder east.
41 Easterlies impinge on the equator that in turn drives surface waters to the west, deepening the
42 thermocline to the west and shoaling it to the east; this allows equatorial upwelling to bring cooler
43 waters on the eastern side. This asymmetry periodically breaks down in the modern-day climate,
44 leading to transient El Niño conditions. Persistent changes to this asymmetry occurred in past
45 climates, leading to the so-called 'permanent El Niño-like' changes. Marked permanent El Niño-
46 like conditions were thought to occur in the Pliocene[1,2], and they have also been proposed to occur
47 at various points in the Quaternary.

48 Understanding past mean changes to the east-west asymmetry is directly relevant to a current
49 debate in tropical Pacific mean state changes under future warming[3]. Virtually all climate models
50 project a pronounced warming in the eastern equatorial Pacific relative to the western equatorial
51 Pacific. However, these projections fly against recent observed trends that show the ***opposite*** to
52 occur, suggesting that the model projections may be in error[3]. This potential error has strong
53 implications for future regional projections of climate. Like interannual El Niño, permanent El-
54 Niño like changes can lead to changes to regional climates throughout the globe mediated through
55 atmospheric teleconnections. Paleoproxy information that documents changes to the tropical
56 Pacific mean climate, in particular its east-west asymmetry, can provide a valuable perspective on
57 this problem.

58 There is currently little consensus on the mean state of the Tropical Pacific during the Little Ice
59 Age (LIA). SST reconstructions indicate relative warming in the eastern[4,5] and central tropical
60 Pacific[6] and cooling in the western equatorial Pacific[7,8], suggesting a more El Niño-like mean
61 state. In contrast, the majority of hydrological records suggest wetter conditions in the western

tropical Pacific[9–13], and drier conditions in the central[14] and the eastern equatorial Pacific[4,15] during the LIA, indicative of a La Niña-like phase during this time. However, a number of records are not consistent with this hydrological trend, either indicating drier (wetter) conditions in western (eastern) equatorial Pacific during the LIA[16,17], or showing no apparent trend[18].

This apparent discrepancy could be explained by other potential drivers of precipitation changes in the tropical Pacific, namely the Intertropical Convergence Zone (ITCZ) and East Asian Summer Monsoon (EASM) and Australian Summer Monsoon (ASM)[14,19]. Presently, it is difficult to differentiate the contribution of the different drivers to shaping the observed paleohydrological patterns during the LIA, because a sufficiently distributed set of paleo proxies that are able to differentiate between these drivers is currently lacking. However, one feature of all these other drivers is that they influence warm-season ***convective*** rainfall. A proxy that primarily measures wintertime orographic rainfall - as we will show for our proxy - would not be as influenced by these various drivers, and thus the climatic interpretation would be less ambiguous.

Here we report a new rainfall record, based on leaf-wax hydrogen isotope data, from a sedimentary sequence from Bulusan Lake (N 12°45', E 124°6') in north-eastern Philippines (Fig. 1-2). The two main sources of rainfall in the area are the western North Pacific (WNP) monsoon, which brings convective rainfall during summer months, and the north-eastern trades (the northern branch of the Australian monsoonal winds) which bring moisture and rainfall during the winter period (SI Appendix Fig. S1a). The latter winter rains deliver the majority of the total annual precipitation to the area, and while the WNP monsoon is operating over this region, its contribution to the annual rainfall amount is smaller. Additionally, typhoons are a prominent source of episodic precipitation, accounting for up to 30% of north-eastern Philippines rainfall in a year[20]. ENSO is the main driver of inter-annual rainfall variability at Bulusan, resulting in reduced (increased) precipitation at Bulusan during El Niño (La Niña) years (SI Appendix Fig. S1b). Consequently, the Bulusan record is ideally suited to provide insights into the mean changes to the east-west asymmetry of the Tropical Pacific climate system during the last millennium.

Results

CHANGES of δD_{wax} IN THE BULUSAN CORE

The top 300 cm from two overlapping sediment cores (BUL1 and BUL2) collected from Bulusan Lake provide a continuous, undisturbed sedimentary sequence spanning the last 1,400 years (Fig. 2d and Fig. S2) (see Methods). An independent and robust age-depth model (Fig. 2c) has been established using 10 AMS^{14}C dates (SI Appendix Table S1 and Section 2). Bulusan sediments contain abundant terrestrial lipid biomarkers, specifically the *n*-alkanes with 27, 29 and 31 carbon atoms ($nC_{27\text{-}31}$) over this time period. We report D/H isotope ratios of those *n*-alkanes (expressed as δ^2H or δD values), as well as an independent record of fossil pollen abundance from the same sedimentary sequence to ensure adequate identification of biomarker sources (Fig. 3) (see Methods).

The $nC_{27\text{-}31}$ alkanes are a major component of the leaf waxes of higher terrestrial plants[21]. δD values of these alkanes (δD_{wax}) in the surface sediments of smaller lakes fed by precipitation and groundwater, such as Bulusan Lake, are significantly correlated with rainfall δD values, offset by a biosynthetic fractionation[22]. δD_{wax} values can be additionally affected by evaporative deuterium enrichment of leaf water due to increased evapotranspiration under low atmospheric humidity[22,23]. At Bulusan, where relative humidity is high year-round, leaf water deuterium enrichment is expected to be minimal[23], and therefore δD_{wax} at the site should faithfully record changes in δD values of precipitation (δD_{precip}).

δD values of the three abundant terrestrial lipid biomarkers, $nC_{27\text{-}31}$, are highly correlated in the Bulusan core, with a coefficient of determination (*r*) ranging between 0.69 and 0.81 ($p<10^{-6}$; SI Appendix Fig. S4), confirming a common origin of these alkanes. The average chain length of *n*-alkanes between nC_{25} and nC_{33} is stable throughout the record up until the 19th century when there is a slight decrease, possibly caused by the changes in the composition of surrounding vegetation due to increasing human activities in the area[24] (SI Appendix Fig. S3b). Fossil pollen

from the same sedimentary sequence reveals that the plant assemblages surrounding the lake during the last 1,400 years contained only a small fraction of grasses (Fig. 3) and were dominated by trees and shrubs (e.g., *Syzygium*, *Elaeocarpus*, *Ficus*, *Macaranga*) (SI Appendix Fig. S5 and Section 6), the likely source of the nC$_{27\text{-}31}$ alkanes[25]. The percentage of grass pollen remained stable between 0-5% throughout the record, indicating that there was no major change in the proportion of C_4 to C_3 plants, and rules out the possibility that vegetation changes have significantly affected δD_{wax} values[22]. However, the nC$_{27}$ alkane (average relative abundance of 20%) in the record shows higher variability in comparison to nC$_{29}$ (average relative abundance of 35%) and nC$_{31}$ (average relative abundance of 45%) indicating more variable sources (Fig. 3). Furthermore, previous studies have suggested that nC$_{31}$ is a major constituent of grasses and herbs[26] in addition to trees[25], which may at least partly explain its reduced variance compared to nC$_{29}$. While δD_{wax} values of all three alkanes show the same pattern, we focus our interpretation on the nC$_{29}$ alkane to minimise the potential distortion of the precipitation signal due to variability in alkane sources and deuterium enrichment differences between C_3 and C_4 plants.

δD values of nC$_{29}$ varied by up to 45‰ during the study period indicating significant hydrological changes at Bulusan Lake over the last 1,400 years (Fig. 3). Relatively low and stable δD_{wax} values occurred during AD 600-1600, followed by a distinct and abrupt increase in δD values at ~AD 1630 (i.e., 20‰ over the period of ~20 years, see SI Appendix Table S2b and Fig. S6, and Section 7). These high δD_{wax} values persisted until ~1900 only to drop just as abruptly to their lowest values in the record over the last 100 years. Based on these elevated δD_{wax} values, we infer El-Niño state conditions during the second half of the LIA (~AD 1630–1900), compared to the rest of the record.

DRIVERS OF PRECIPITATION δD VALUES AT BULUSAN

We use a range of instrumental datasets and global circulation model outputs to identify drivers of δD_{wax} (and therefore δD_{precip}) variations at Bulusan, using the interannual variability to isolate

enriched and depleted years. First, we use an isotope-enabled general circulation model (isoGSM2; see Methods) to understand the large-scale drivers of δD_{precip} values in the north-eastern Philippines. Since the northeastern Philippines is spatially too limited for the rainfall to be adequately resolved in isoGSM2, we analyze instead the δD of precipitable water (hereafter δD_{pw}) for the isoGSM2 gridpoint closest to that region (N 13°, E 124°); variations in δD_{pw} are found to closely match variations in the δD of station rainfall measured over that region (SI Appendix Fig. S7, Table S3). We generate an interannual index of amount-weighted δD_{pw} (using July and the following June as the start and end months) and compare years with enriched δD_{pw} with depleted years (Fig. 4a). There is a clear El Niño influence for enriched years – the 1982-83, 1997-98 and 2015-16 El Niños stand out (Fig. 4a), and moreover the amount-weighted δD_{pw} index is correlated with an interannual index of ENSO (Nino3.4 averaged over the peak months of Oct-Feb, Fig. 5a) at $r = 0.75$ ($p<0.001$; Fig. 4b). Years with more positive δD_{pw} values are drier over the northern Philippines during the winter rainfall months (October-February), because of reduced moisture flux from the northeasterly trades impinging on the northeastern Philippines (Fig. 4c and d).

To further assess the influence of ENSO on δD_{pw} at Bulusan, we composite δD_{pw} of El Niño and La Niña years over the Bulusan gridpoint (N 13°, E 124°) and find that precipitable water is heavier (lighter) during El Niño (La Niña) years compared to neutral ENSO years, in particular over the winter and spring months (Fig. 5b). Despite being highly negative and a mismatch in absolute values, as they are averaged for the entire atmospheric column of water vapor, the relative change between El Niño and La Niña years in modelled δD_{pw} values of about 11‰ is consistent with surface water observations[27]. Regionally, precipitable water is isotopically enriched over the western Tropical Pacific and Maritime continent for El Niño years relative to La Niña years (SI Appendix Fig. S8), accompanying the El Niño-driven reduction to rainfall over those regions. The two are causally related: El Niño reduces deep convection over the western tropical Pacific, and since convection depletes the isotopic composition of water vapor, water vapor in this region becomes isotopically enriched (SI Appendix Fig. S8).

Similarly, differences in precipitation amount at Bulusan also occur during the winter months between El Niño and La Niña years. Observed rainfall from the Climate Research Unit TS version 4.03[28] dataset for the gridpoint nearest Bulusan (N 12°45', E 124°15') (see Methods) show that La Niña years has more precipitation than neutral ENSO years, and El Niño years has less (Fig. 5c). A similar relationship for precipitation and δD_{precip} can be observed in the Global Network of Isotopes in Precipitation (GNIP) data (SI Appendix Fig. S9), where the major difference between 1997 and 1998 years is during the winter.

Our results demonstrate that δD_{pw} (and therefore also δD_{wax}) values are isotopically enriched, and rainfall is reduced, during El Niño years relative to La Niña years. The bulk of the rainfall changes occur during the winter months (October-March). This relationship to ENSO allows us to use Bulusan δD to monitor past changes in the east-west asymmetry of the equatorial Pacific climate.

Discussion

Based on our analysis above, the distinct and abrupt increase in nC$_{27-31}$ alkane δD values in the Bulusan paleorecord between ~AD 1630-1900 suggests an abrupt shift in the hydroclimate of the western tropical Pacific during the late LIA towards significantly drier conditions. Since the lowland tropics are characterized by low temperature variability during the Holocene[4,18,29], the 'temperature effect' on the isotopic composition of precipitation in these regions should be negligible[22], and is therefore not normally included in the interpretation of the δD changes in the paleorecords from the tropical Pacific from this time period.

While several paleohydrological records from the region have had the changes in their isotopic signatures linked to shifts in the geographic position and extent of ITCZ[14,19], our isoGSM2 analysis confirms that Bulusan δD is a wintertime rainfall proxy, and provides no indication of an association between ITCZ/ monsoon dynamics and present-day precipitation δD values. Instead, our results indicate that ENSO is the key driver of present-day precipitation δD variations at Bulusan, as the decrease in convective activity over the western tropical Pacific during El Niño

189 years leads to an enrichment of water vapor in the region (SI Appendix Fig. S8). Furthermore,
190 while previous interpretations of changes in precipitation stable isotopes in the region have
191 focused on precipitation amount, our findings are supported by several recent studies which have
192 suggested that ENSO can directly influence precipitation stable isotopic values on an interannual
193 scale via alterations in the strength of convective activity across the tropics (e.g.[30–32]).
194 Additionally, a number of studies have demonstrated a mismatch between local precipitation and
195 precipitation stable isotopes in the western tropical Pacific[33–36], instead implicating factors beyond
196 the amount effect such as vapor transport history and the degree of vapor parcel distillation.
197 Therefore, the variability in precipitation stable isotopes in the western tropical Pacific seem to be
198 reflective of regional-scale atmospheric circulation rather than local rainfall amount.

199 Based on our modern climate system results showing ENSO having a dominant role in shaping
200 inter-annual precipitation δD dynamics at Bulusan, we propose that the establishment of an El
201 Niño-like mean state conditions in the tropical Pacific during the LIA was responsible for the
202 hydrological changes recorded in the Bulusan paleorecord. The reduction in the east-west
203 asymmetry in the tropical Pacific mean state results in a reduced Walker circulation, leading to
204 drier conditions over the western Pacific similar to what occurs during El Niño conditions today.
205 Similarly, there would also be changes to the structure of convection in the tropical Pacific
206 whereby the ITCZ of the northern tropical Pacific and the South Pacific Convergence Zone
207 (SPCZ) collapses to a single ITCZ near the equator in the western and central equatorial Pacific,
208 similar to what is seen during strong El Niño events today[37]. In the eastern Pacific, the northern
209 ITCZ shifts equatorwards as well. Consequently, a shift in the geographic location of the ITCZ
210 and a shift to a more El Niño-like mean state conditions are not necessarily at odds and may have
211 actually been causally linked in the past. Therefore, our results do not challenge that a shift in the
212 geographic position and/ or extent of ITCZ and monsoonal belt have taken place during LIA, but
213 rather suggest that the changes in these climatic phenomena is not something that Bulusan δD
214 proxy monitors.

Our results are supported by SST-based records from the tropical Pacific. The period of El Niño-like mean state conditions, inferred from the Bulusan record, corresponds to the period of relative warming in the eastern[4,5] and central tropical Pacific[6] and further cooling in the western equatorial Pacific[7,8] during the LIA, also interpreted as an El Niño-like mean state conditions (Fig. 6). While several paleohydrological records from the region indicate the opposite situation, i.e., wetter conditions in the western Pacific[9–13], and drier conditions in the central[14] and the eastern Pacific[4,15] during the LIA, other records indicate a trend of decreasing precipitation in the western Pacific (i.e., Makassar Strait[9]) and increased precipitation in the eastern Pacific (i.e., Poza de la Diablas[16]) between AD 1600 and 1900, which further supports our interpretation. Arguably the strongest support from the tropical Pacific for our results comes from the Palau's Clear Lake δD record[17], located close to the Bulusan site, which also suggests drier conditions during this time (i.e., AD 1580-1820). Tierney *et al*.[38] offer additional support from a remote location with strong climatic connections to ENSO today. The authors argued that the East African hydrological changes formed part of a larger tropics-wide climate change linked to warmer SSTs in the western Indian Ocean and cool SSTs in the eastern Indian Ocean and western Pacific warm pool, analogous to what is seen from teleconnections during El Niño events in present-day climate. The timing and nature of the East African hydrological changes match those seen in the Bulusan record, consistent with the onset of El Niño-like mean state conditions.

Absence of externally forced background climate changes during the last millennium would suggest that the 1630-1900 AD event marked by El Niño-like mean state conditions was most likely caused by internal variability of the tropical Pacific climate system. Various means by which ENSO may influence the tropical Pacific mean state, and vice versa, have been previously described[39–46], highlighting how the relationship between the tropical Pacific mean state and ENSO variability is complex and interactive[47–49]. An alternative explanation to the changes in the tropical Pacific mean state is volcanic forcing via ENSO. The influence of volcanic activity on ENSO has been widely demonstrated, with most observations (e.g.,[50,51]) and paleoclimate records

(e.g.,[52–55]), as well as several modelling studies, suggesting that major tropical volcanic eruptions give rise to El Niño events[55–62]. Thus, one can imagine how the increased volcanic activity during LIA[63,64] may have amplified El Niño activity, and subsequently, caused or contributed to El Niño-like mean state conditions.

A reduction in δD_{wax} values around 1900 AD suggests an onset of La Niña-like mean state conditions in the equatorial Pacific. This is in congruence with instrumental data which record a continued strengthening of the zonal SST gradient in recent decades, along with a sharp increase in the greenhouse gas (GHG) concentrations[65]. In contrast, state-of-the-art climate models predict that rising GHGs decrease the SST gradient across the tropical Pacific[65]. This striking mismatch between models and observational data has been recently explored by Seager *et al.* (2019)[3], who attribute the erroneous model response to a well-known cold bias in the Pacific cold tongue as simulated by the coupled models. The Bulusan record provides a longer perspective on this question, indicating that La Niña-like trend in tropical Pacific SSTs may have taken started as early as early 1900s, though the low resolution of the age-depth model in the top section of the core hinders a more exact timing of the onset of this trend. Nevertheless, our results highlight the potential of paleorecords for informing the question of recent changes in the TP mean state climate in response to the rising GHGs.

A remarkable feature of our record is the abrupt transition from low to high δD_{wax} values between 1600 and 1650. This suggests that marked changes to the tropical Pacific mean state asymmetry can occur on decadal timescales. The shift from a strong to a weak zonal gradient recorded at the Bulusan site happened over the period of only ~20 years, as did the subsequent return to the strong gradient ~270 years later. This finding is in accordance with SST-based zonal gradient reconstructions from the region. For instance, Conroy *et al.* 2010[5] found that a change to a state of weak zonal gradient of tropical Pacific SST at ~AD 1650, interpreted as an onset of El Niño-like conditions, happened over the course of a few decades, very similar to the hydrological shifts recorded in the Bulusan record. Despite the increasing paleo-evidence, current fully coupled

climate models do not reproduce such abrupt shifts in tropical Pacific mean state, underlining potential limits in our mechanistic understanding.

Overall, although the evidence presented in our study originates from a single site, our data, combined with other relevant paleohydrological records from the region and modern observational and modelling data, make a strong case for a rapid transition to an El Niño-like mean state during the second half of the LIA and subsequent reduction in precipitation amount. Our findings emphasize the prominent role of the tropical Pacific ocean-atmosphere mean climate, particularly its east-west asymmetry, in shaping precipitation patterns in the tropical Pacific over the past millennium through regionally rapid, decadal changes in its mean state. Through atmospheric teleconnections, these changes could have then be communicated globally to shift regional climates elsewhere, akin to what happens during an ENSO event today.

Materials and Methods

I. ***Paleoclimate system***

Study site and material collection. Bulusan Lake is a 0.28 km^2 oval shaped lake located at 360 m.a.s.l., at the foot-slopes of Mount Bulusan volcano at the southeast end of the Bicol Volcanic Arc[66]. It consists of two basins: a small round basin, and a larger narrow basin, which are 12 and 24 meters deep respectively. The two basins comprise a closed system fed primarily by precipitation and groundwater. The vegetation surrounding Bulusan Lake, and up the slope of Mt Bulusan, is classified as a Dipterocarp rainforest, i.e., aseasonal lowland tropical rainforest dominated by the Dipterocarpaceae tree family[24]. Two overlapping sedimentary sequences, 5.3 m BUL1 and 5.0 m BUL2, were collected as 1 m segments from the smaller basin with a Livingstone Piston corer using an anchored platform in March 2013. The sediments were sealed in protective plastic containers and shipped to the University of Oxford where they have been stored at 5 °C.

Age-Depth Modelling. A robust age-model for the Bulusan sediments has been established with AMS^{14}C dates (Table S1) and the surface sediment set to 2013 (the year the core was collected). The radiocarbon analysis was done on identified terrestrial plant macrofossils (e.g., leaves, twigs) to avoid reservoir effects and minimize age uncertainty. AMS^{14}C samples were measured at the NERC Radiocarbon Facility, East Kilbride. The age-depth modelling of the Bulusan core was performed using a Bayesian statistics approach to reconstruct accumulation histories for deposits with the Bacon 2.2 package in R[67,68] at 1 cm resolution and the IntCal13 radiocarbon calibration curve for the Northern Hemisphere[69], and model output estimates the age span per cm being between 4.5-6 years. For further details, see SI Appendix Section 2.

Biomarker extraction, identification, and quantification. Sediment samples were sampled at the University of Oxford as a continuous series of 4 cm long slices (i.e., 2-6 g dry weight per sample) from a 300 cm long sequence, with each slice corresponding to a ~20-year interval. The samples were freeze-dried, and lipid biomarkers extracted at the University of Potsdam with a

dichloromethane (DCM): methanol mixture (9:1) at 100 °C and 103 bar using a Dionex accelerated solvent extraction system (ASE) 350. The extracts were separated into aliphatic and aromatic/alcohol/fatty acid fractions by solid phase extraction (SPE) in 8 ml glass columns filled with 2 g silica gel (0.040 mm to 0.063 mm mesh size) using hexane and DCM: methanol mixture (9:1) for elution, respectively, for a detailed description see the manual SPE extraction procedure in Rach *et al*. 2020[70].

The *n*-alkanes ($nC_{23\text{-}33}$ homologues) from the aliphatic fraction were identified and quantified at the University of Potsdam using a gas chromatograph (Agilent GC 7890-A) equipped with a mass selective detector-mass and a flame ionisation detector (FID) (Agilent MS 5975-C) coupled via an electronic split interface. The MSD trace was employed for compound identification. Peak area from the FID chromatogram was used for compound quantification by calibrating against the peak area of the internal standard 5α-androstane. Sulphur and unsaturated hydrocarbons were removed from the aliphatic fraction by elution through a pipette column of activated copper powder and a pipette column of activated mix of silver nitrate and silica gel, respectively, by applying a combination of hexane and dichloromethane (DCM). The resulting aliphatic fraction produced clean chromatograms and no unresolved complex mixture (UCM) was detected (except in Samples 1-6).

Compound-specific hydrogen isotope measurement of n-alkanes. Compound-specific hydrogen isotope ratios of the aliphatic fraction were measured at the University of Potsdam using a ThermoFisher Delta-V-Plus Isotope Ratio Mass Spectrometer coupled to a ThermoFisher TraceGC 1310 gas chromatograph. The samples were measured on a 50 m HP ultra 1 column with an inner diameter of 0.2 mm and a film thickness of 0.33 μm. The samples were measured with the following GC-temperature program: i) temperature was held for 2 mins at 40 °C, i) temperature was increased to 256 °C at a rate of 4 °C per min, iii) oven temperature was increased to 300 °C at 2 °C per min, and iv) the final temperature was held for 45 mins. The alkane standard mix was measured with a shorter program where the final temperature of 300 °C was held for 3

329 mins only, as all standard peaks had eluted. The samples were measured in triplicates, except for
330 top 6 samples which were measured in duplicates due to low compound concentrations.

331 A standard containing nC$_{16}$ to nC$_{30}$ alkanes with known δD values (mix A4, Arndt
332 Schimmelmann, University of Indiana) was measured in duplicate at the beginning and the end of
333 each sequence or after six sample injections, and then used for normalisation of δD values to the
334 Vienna Standard Mean Ocean Water (VSMOW) scale. The mean standard deviation of all
335 measured samples for the nC$_{27}$, nC$_{29}$ and nC$_{31}$ alkanes (n=75) was about 1.6‰, 1.3‰ and 0.9‰,
336 respectively. The H3+ factor was determined once a day and remained constant over the
337 measurement period, indicating stable ion source conditions.

338 ***Isotope evaluation.*** Compounds with intensities below 800 mV (on mass 2) (i.e., nC$_{23}$ and nC$_{25}$)
339 were not used for evaluation, since this was outside of the linear range of the GC-IRMS system. In
340 addition, an exclusively higher terrestrial plant origin of nC$_{25}$ is difficult to assume because the
341 alkane can be produced by aquatic plants such as *Potamogeton*. Therefore, for our interpretations
342 we only used δD values of alkanes with 27, 29 and 31 carbon atoms (nC$_{27\text{-}31}$), which showed
343 clean, baseline separated peaks in all samples (except nC$_{31}$ in Sample 2 which coeluted with an
344 unidentified substance). The nC$_{27\text{-}31}$ alkanes are the most widely used leaf wax biomarkers and
345 their hydrogen isotopic composition has been shown as a robust recorder of plant source water δD
346 along extraordinarily steep climatic gradients[21].

347 ***Extraction and processing of fossil pollen.*** Sediment samples were extracted as a continuous
348 series of 4 cm long 1 cm^3 slices from the top 3.0 m of the composite Bulusan core, with each slice
349 corresponding to a ~20-year interval. Standardised protocols were employed for the extraction and
350 processing of fossil pollen from the sediment samples[71]. 500 terrestrial pollen grains were counted
351 in each sample (and identified to family or genus level where possible, Fig. S5), and the relative
352 abundance of grass and sedge taxa at each level was calculated as the proportion of grass and
353 sedge pollen in the total terrestrial pollen counts (expressed in percentages), at the same extent and

resolution as the δD_{wax} records.

II. Modern climate system

Rainfall Data. We use the Climate Research Unit gridded Time Series version 4.03 dataset (CRU TSv4)[28] of monthly mean climatic quantities. Individual station rainfall data are combined and gridded onto a 0.5 degree horizontal grid using angular distance weighting. We use the gridpoint closest to Bulusan lake position (N 12°45', E 125°15'), to represent the rainfall over that region. We also only use the time period overlapping with the isoGSM2 data, from 1979 to 2017.

Isotope-incorporated Global Spectral Model version 2 (IsoGSM2) simulation of precipitation isotopes. Output from an isotope-enabled general circulation model, the isoGSM version 2[72] between 1979 to 2017, is used in this study. IsoGSM2 is based on a version of the Scripps Experimental Climate Prediction Center's global spectral model, but with the large-scale fields nudged towards the National Center for Environmental Prediction version 2 (NCEP2) reanalyses[72,73]. Nudging is done for temperature, zonal and meridional winds only, and only for large (>1000km) spatial scales. In this respect, the isoGSM2 simulation is similar to NCEP2, but with the addition of precipitation isotopes. The simulated precipitation isotopes have been shown to be realistic when compared to observations[74]; however, because of the relatively coarse horizontal resolution of isoGSM2 (T62, corresponding to 1.89 degrees at the equator), north-eastern Philippines rainfall is not adequately resolved. In lieu of using precipitation isotopes from isoGSM2, we use the simulated δD of precipitable water (δD_{pw}) at the gridpoint closest to Bulusan lake to assess changes to the δD of rainfall. The underlying assumption here is that changes to δD of rainfall reflect changes to the δD of vapor supplying the rainfall. We support this assumption by showing that changes in the simulated δD_{pw} compared favourably with observed δD measured by GNIP (see SI Appendix Fig. S7 and Section 8).

ENSO analysis. We derive an interannual index of ENSO by taking the average of sea surface temperature monthly anomalies over the Nino3.4 region (5S-5N, 170W-120W), and then

379 averaging over the ENSO peak months of October through February; the index is subsequently
380 referred to as Nino3.4ONDJF. To obtain the El Niño and La Niña composites for Fig. 5, we define
381 years where Nino3.4ONDJF > 0.7 as El Niño years, and Nino3.4ONDJF < -0.7 as La Niña years.

382 **Acknowledgments**

383 **General:** We thank the Philippine Bureau of Fisheries and Aquatic Resources and the Philippine
384 Department of Environment and Natural Resources, as well as the Bulusan Volcano Natural Park
385 staff, for permitting and facilitating our research at the Bulusan Lake. We would also like to thank
386 Professor Keith Bennett (University of St Andrews) and Philip Bartilet (Bulusan Volcano Natural
387 Park) for fieldwork assistance, and Iris Van Der Veen (University of Potsdam) and Anne Thoisen
388 (University of Aarhus) for laboratory assistance. For assistance with the figures, we thank Marwan
389 Butrous. Finally, we thank Kei Yoshimura for providing access to isoGSM2 data. **Funding:** This
390 work was supported by Royal Geographical Society (Monica Cole Research Grant and Paddy
391 Coker Postgraduate Research Award), Quaternary Research Association (New Research Worker's
392 Award), Department of Zoology at the University of Oxford (Postgraduate Research and Training
393 Grant), and Merton College (Graduate Research Expenses and Supplementary Travel Grants).
394 Radiocarbon dating was funded by the Natural Environment Research Council. A.P. was
395 supported by the Clarendon Fund. D.S. was supported by an Emmy-Noether grant of the DFG
396 (SA-1889/1) and an ERC Consolidator grant (STEEPclim, Grant agreement no.: 647035). **Author**
397 **contributions:** A.P. initiated and designed the study, collected lake sediments, co-acquired
398 financial support, carried out the data analysis and interpretation, and co-wrote the paper.
399 A.W.R.S., J.C.H.C. and B.M. contributed to the data analysis and paper writing, and A.W.R.S.
400 and J.C.H.C. were also involved in data interpretation. K.J.W. contributed to paper writing and
401 acquired financial support. D.S. contributed to study design, co-acquired financial support, co-
402 interpreted the results, and co-wrote the paper. **Competing interests:** The authors declare that
403 they have no competing interests. **Data and materials availability:** All data needed to appraise
404 the conclusions in the paper are given in the Main Text and/ or the Supplementary Materials. The

Nino3.4 index was taken from NOAA Physical Sciences Laboratory (NOAA PSL): https://psl.noaa.gov/data/climateindices/list/. Any additional data related to this paper may be requested from the authors.

Figures

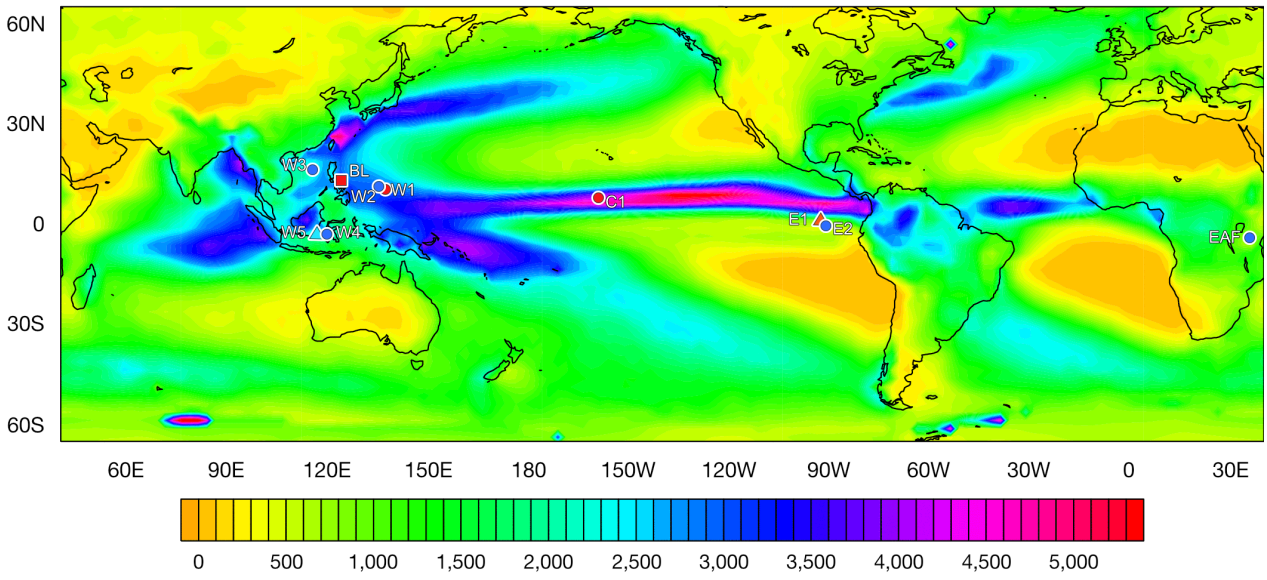

Fig. 1. Map of mean annual precipitation in the tropical Pacific showing the location of our study site, Bulusan Lake (BL, square) and the locations of other hydrological (circles) and sea surface temperature records (triangles). In the western Pacific, Clear Lake (W1)[17] and Spooky Lake (W2)[14] in Palau Island, Dongdao Island (W3)[12], and Makassar Strait (W4[9], W5[7,8]). In the central Pacific, Washington Island (C1)[14], and in the eastern Pacific, El Junco Lake (E1)[4] and Poza de la Diablas (E2)[16] in the Galapagos Islands. Overall wetter and drier conditions derived from the mapped records (circles, triangles) are depicted in blue and red, respectively. The band of heavy precipitation indicates the ITCZ. Modified figure from Wallace *et al.*[75].

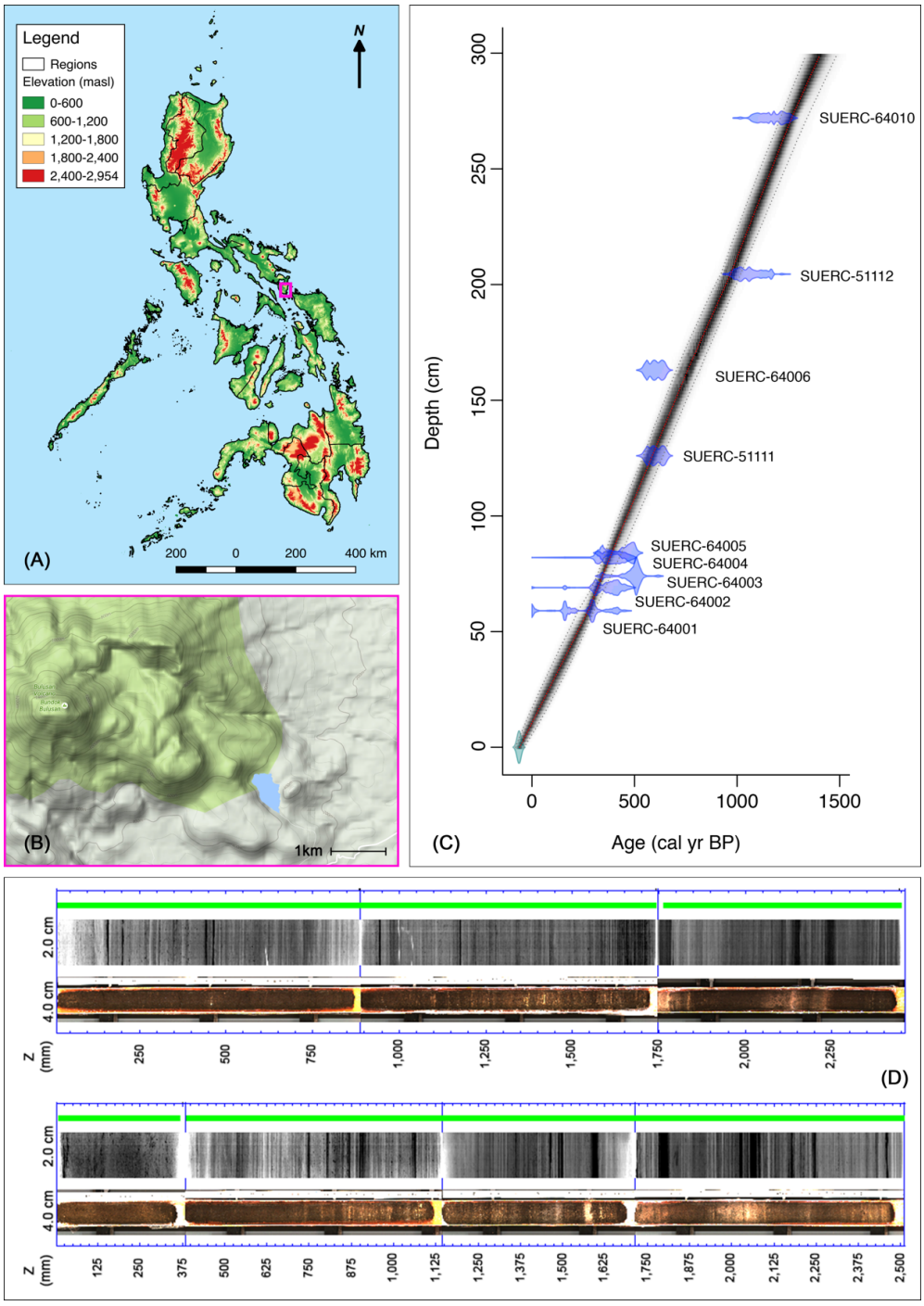

418

419 **Fig. 2. Geographical and sedimentological features of the Bulusan site. (A),** Topographic map of the
420 Philippines showing the location of the Bulusan site. Data from PhilGIS[76], map generated in QGIS version
421 2.14.3[77]. **(B)**, Map showing Bulusan Lake (blue) within its larger landscape, with Mt Bulusan volcano in the
422 west (green)[78]. **(C)**, Age-depth model for the Bulusan sediment sequence, constructed with *Bacon 2.2* [67,68] in
423 R version 3.2.4[79]. Probability distributions for the radiocarbon dates are shown in blue. The top of the
424 sediment sequence is assigned the year the cores were collected. The shaded areas represent the 1σ probability
425 age ranges by interpolating between ^{14}C age control points. The red dashed line represents the age-depth
426 calibration used in further analysis. SUERC-64011 not shown here as it lies below the analysed section. **(D)**,
427 Optical and radiograph profiles of the Bulusan sediments, generated in ItraxPlot program[80]. The radiograph
428 images depict the level of organic content, with higher values shown as lighter bands. The green line
429 represents the validation of the measurement quality along the cores. For more details on the physical and
430 chemical characterisation of Bulusan cores, see SI Appendix Section 1.

Fig. 3. Paleorecords from the Bulusan Lake. A record of H/D isotope ratio measurements of leaf wax alkanes (nC$_{27\text{-}31}$), expressed as δD values with error bars of 1 standard deviation, and a record of fossil pollen abundance expressed as the percentage of grasses (Poaceae) and sedges (Cyperaceae), representing C4 plants, vs. other terrestrial plant taxa, predominantly trees and shrubs, representing C3 plants. Data plotted with *ggplot2* package[81] in R version 3.2.4[79].

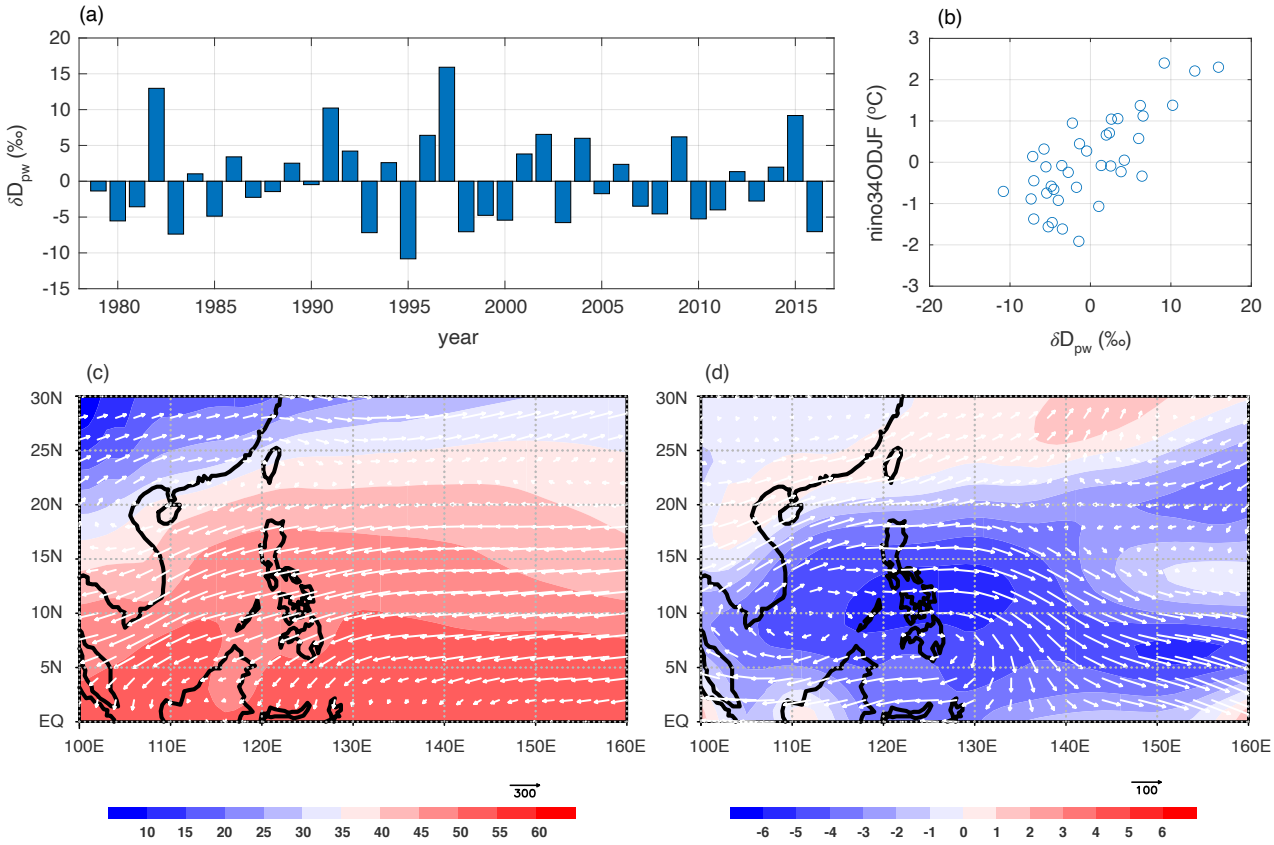

Fig. 4. Examination of δD values of precipitable water (δD_{pw}) of enriched vs. depleted years using isoGSM2 output. (a) Time Series of the amount-averaged δD_{pw} over Bulusan, and correlation. δD at the gridpoint closest to Bulusan was amount-averaged from the preceding July through following June. The mean (-151.23 per mil) was subtracted and the timeseries detrended prior to plotting. Years with high δD_{pw} are enriched. **(b)** Scatterplot between the amount-weighted δD_{pw} with an interannual index of ENSO (Nino3.4 averaged over the peak months of Oct-Feb. The two time series are correlated at r=0.75 ($p<0.001$). **(c)** Climatological vertically-integrated moisture flux during the northern Philippines wet months of October-Feb (vectors; reference vector is 300 (g/kg).(m/s)), and the Oct-Feb precipitable water (shaded; units are kg/m^2). **(d)** Difference in the vertically-integrated moisture flux (vectors; reference vectors is 100 (g/kg).(m/s)) and precipitable water (shaded; units are kg/m) averaged over Oct-Feb, enriched minus depleted years; the eight most enriched years in **(a)** are used for the enriched composite; similarly for depleted years. For enriched years, there is reduced moisture flux by the north-easterly trades into the northern Philippines.

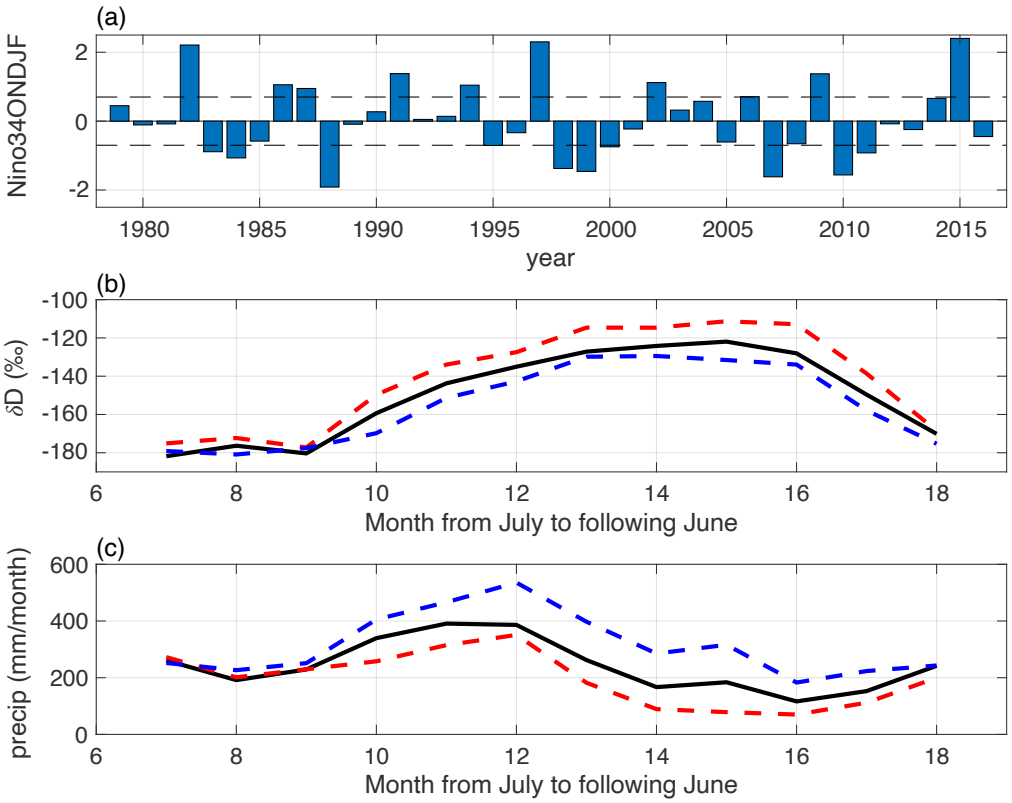

Fig. 5. Relationship between ENSO, precipitation, and precipitable water δD at Bulusan. (a) Nino3.4 averaged over Oct-Feb which we use as an interannual index of ENSO. We use +0.7K as the threshold to identify El Niño years, and -0.7K for La Niña years (horizontal dashed lines); the remainder of the years are neutral years. **(b)** δD of precipitable water for the El Niño (red), neutral (black) and La Niña (blue) composites at Bulusan. Here, we use the isoGSM2 gridpoint nearest Bulusan lake (N 13°, E 124°) for the δD field. **(c)** Precipitation for the El Niño (red), neutral (black) and La Niña (blue) composites at Bulusan. Here, we use the CRU TS v4 rainfall gridpoint closest to Bulusan lake, at N 12°45', E 124°15' (see Methods). Together, **(a)** and **(c)** shows that rainfall is reduced, and isotopically heavier, for El Niño years.

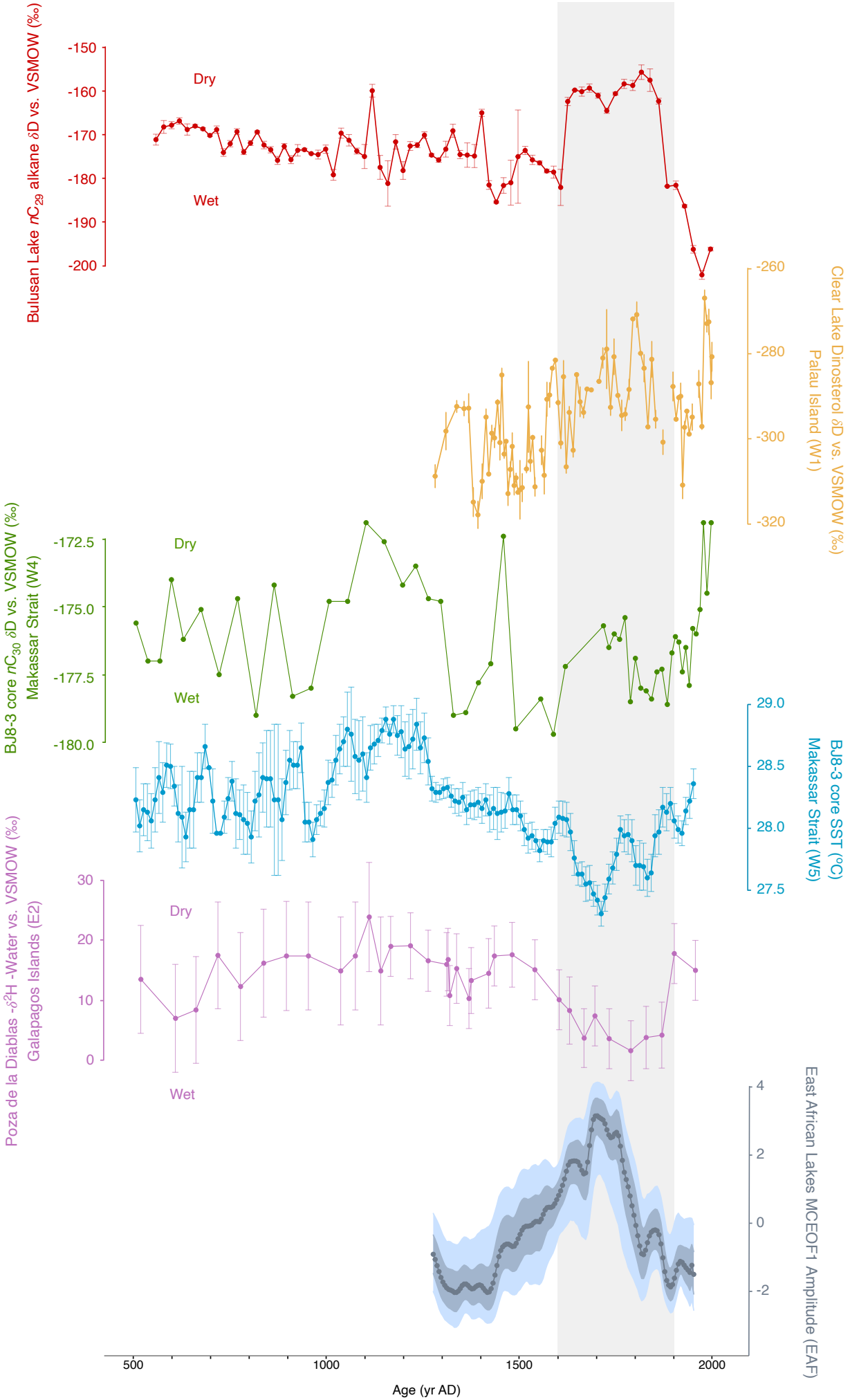
Bulusan Lake nC_{29} alkane δD vs. VSMOW (‰)
-150
-160
-170
-180
-190
-200
Dry
Wet
Clear Lake Dinosterol δD vs. VSMOW (‰)
Palau Island (W1)
-260
-280
-300
-320
BJ8-3 core nC_{30} δD vs. VSMOW (‰)
Makassar Strait (W4)
-172.5
-175.0
-177.5
-180.0
Dry
Wet
BJ8-3 core SST (°C)
Makassar Strait (W5)
29.0
28.5
28.0
27.5
Poza de la Diablas -δ^2H -Water vs. VSMOW (‰)
Galapagos Islands (E2)
30
20
10
0
Dry
Wet
East African Lakes MCEOF1 Amplitude (EAF)
4
2
0
-2
500
1000
1500
2000
Age (yr AD)

463

Fig. 6. Comparison of the Bulusan record (nC$_{29}$ alkane δD values) with other paleohydrological and SST records. In the western Pacific, Clear Lake (W1)[17] and Makassar Strait (W2, W4)[7,89], in the eastern Pacific, Poza de las Diablas (E2)[16], and in the East Africa Lakes MCEOF record (EAF)[38]. Data plotted with *ggplot2* package[81] in R version 3.2.4[79]. Grey strip denotes the period of significant change in the Bulusan record (~AD 1600-1900).

REFERENCES

1. Wara, M. W., Ravelo, A. C. & Delaney, M. L. Permanent El Niño-like conditions during the Pliocene warm period. *Science* **309**, 758–761 (2005).
2. Fedorov, A. V. *et al.* The Pliocene paradox (mechanisms for a permanent El Niño). *Science* **312**, 1485–1489 (2006).
3. Seager, R. *et al.* Strengthening tropical Pacific zonal sea surface temperature gradient consistent with rising greenhouse gases. *Nat. Clim. Chang.* **9**, 517–522 (2019).
4. Conroy, J. L., Overpeck, J. T., Cole, J. E., Shanahan, T. M. & Steinitz-Kannan, M. Holocene changes in eastern tropical Pacific climate inferred from a Galápagos lake sediment record. *Quaternary Science Reviews* vol. 27 1166–1180 (2008).
5. Overpeck, J. T. & Cole, J. E. El Niño/Southern Oscillation and changes in the zonal gradient of tropical Pacific sea surface temperature over the last 1.2 ka. *PAGES news* vol. 18 32–34 (2010).
6. Cobb, K. M., Charles, C. D., Cheng, H. & Lawrence Edwards, R. El Niño/Southern Oscillation and tropical Pacific climate during the last millennium. *Nature* vol. 424 271–276 (2003).
7. Newton, A., Thunell, R. & Stott, L. Climate and hydrographic variability in the Indo-Pacific Warm Pool during the last millennium. *Geophysical Research Letters* vol. 33 (2006).
8. Oppo, D. W., Rosenthal, Y. & Linsley, B. K. 2,000-year-long temperature and hydrology reconstructions from the Indo-Pacific warm pool. *Nature* vol. 460 1113–1116 (2009).
9. Tierney, J. E., Oppo, D. W., Rosenthal, Y., Russell, J. M. & Linsley, B. K. Coordinated hydrological regimes in the Indo-Pacific region during the past two millennia. *Paleoceanography* vol. 25 (2010).
10. Rodysill, J. R. *et al.* A paleolimnological record of rainfall and drought from East Java, Indonesia during the last 1,400 years. *Journal of Paleolimnology* vol. 47 125–139 (2012).
11. Zeng, Y. *et al.* The wet Little Ice Age recorded by sediments in Huguangyan Lake, tropical South China. *Quaternary International* vol. 263 55–62 (2012).
12. Yan, H. *et al.* South China Sea hydrological changes and Pacific Walker Circulation variations over the last millennium. *Nature Communications* vol. 2 (2011).
13. Konecky, B. L. *et al.* Intensification of southwestern Indonesian rainfall over the past millennium. *Geophysical Research Letters* vol. 40 386–391 (2013).
14. Sachs, J. P. *et al.* Southward movement of the Pacific intertropical convergence zone AD 1400–1850.

Nature Geoscience vol. 2 519–525 (2009).

15. Moy, C. M., Seltzer, G. O., Rodbell, D. T. & Anderson, D. M. Variability of El Niño/Southern Oscillation activity at millennial timescales during the Holocene epoch. *Nature* vol. 420 162–165 (2002).
16. Nelson, D. B. & Sachs, J. P. Galápagos hydroclimate of the Common Era from paired microalgal and mangrove biomarker 2H/1H values. *Proceedings of the National Academy of Sciences* vol. 113 3476–3481 (2016).
17. Richey, J. N. & Sachs, J. P. Precipitation changes in the western tropical Pacific over the past millennium. *Geology* vol. 44 671–674 (2016).
18. Griffiths, M. L. *et al.* Younger Dryas–Holocene temperature and rainfall history of southern Indonesia from δ18O in speleothem calcite and fluid inclusions. *Earth and Planetary Science Letters* vol. 295 30–36 (2010).
19. Yan, H. *et al.* Dynamics of the intertropical convergence zone over the western Pacific during the Little Ice Age. *Nature Geoscience* vol. 8 315–320 (2015).
20. Rodgers, E. B., Adler, R. F. & Pierce, H. F. Contribution of Tropical Cyclones to the North Pacific Climatological Rainfall as Observed from Satellites. *Journal of Applied Meteorology* vol. 39 1658–1678 (2000).
21. Eglinton, G. & Hamilton, R. J. Leaf Epicuticular Waxes. *Science* vol. 156 1322–1335 (1967).
22. Sachse, D. *et al.* Molecular Paleohydrology: Interpreting the Hydrogen-Isotopic Composition of Lipid Biomarkers from Photosynthesizing Organisms. *Annual Review of Earth and Planetary Sciences* vol. 40 221–249 (2012).
23. Kahmen, A. *et al.* Leaf water deuterium enrichment shapes leaf wax n-alkane δD values of angiosperm plants II: Observational evidence and global implications. *Geochimica et Cosmochimica Acta* vol. 111 50–63 (2013).
24. E. Abada Gatumbato, W. Carandang, N. Pampolina, N. A. Mallar, S. Narvadez. *Final Report: Physical and Geopolitical Characteristics, Biological Resources, Socio-Cultural and Economics Conditions and Institutional Arrangements/Governance of the Bulusan Volcano Natural Park*. (2011).
25. Feakins, S. J. *et al.* Production of leaf wax n-alkanes across a tropical forest elevation transect. *Organic Geochemistry* vol. 100 89–100 (2016).

26. Schwark, L., Zink, K. & Lechterbeck, J. Reconstruction of postglacial to early Holocene vegetation history in terrestrial Central Europe via cuticular lipid biomarkers and pollen records from lake sediments. *Geology* vol. 30 463 (2002).
27. Lee, J.-E. *et al.* Asian monsoon hydrometeorology from TES and SCIAMACHY water vapor isotope measurements and LMDZ simulations: Implications for speleothem climate record interpretation. *Journal of Geophysical Research: Atmospheres* vol. 117 (2012).
28. Harris, I., Osborn, T. J., Jones, P. & Lister, D. Version 4 of the CRU TS monthly high-resolution gridded multivariate climate dataset. *Sci Data* **7**, 109 (2020).
29. van Breukelen, M. R., Vonhof, H. B., Hellstrom, J. C., Wester, W. C. G. & Kroon, D. Fossil dripwater in stalagmites reveals Holocene temperature and rainfall variation in Amazonia. *Earth and Planetary Science Letters* vol. 275 54–60 (2008).
30. Cai, Z. & Tian, L. Atmospheric Controls on Seasonal and Interannual Variations in the Precipitation Isotope in the East Asian Monsoon Region. *Journal of Climate* vol. 29 1339–1352 (2016).
31. Gao, J., He, Y., Masson-Delmotte, V. & Yao, T. ENSO Effects on Annual Variations of Summer Precipitation Stable Isotopes in Lhasa, Southern Tibetan Plateau. *Journal of Climate* vol. 31 1173–1182 (2018).
32. Hurley, J. V., Vuille, M. & Hardy, D. R. On the Interpretation of the ENSO Signal Embedded in the Stable Isotopic Composition of Quelccaya Ice Cap, Peru. *Journal of Geophysical Research: Atmospheres* vol. 124 131–145 (2019).
33. Cobb, K. M., Adkins, J. F., Partin, J. W. & Clark, B. Regional-scale climate influences on temporal variations of rainwater and cave dripwater oxygen isotopes in northern Borneo. *Earth and Planetary Science Letters* vol. 263 207–220 (2007).
34. Kurita, N., Ichiyanagi, K., Matsumoto, J., Yamanaka, M. D. & Ohata, T. The relationship between the isotopic content of precipitation and the precipitation amount in tropical regions. *Journal of Geochemical Exploration* vol. 102 113–122 (2009).
35. Moerman, J. W. *et al.* Diurnal to interannual rainfall δ18O variations in northern Borneo driven by regional hydrology. *Earth and Planetary Science Letters* vols 369-370 108–119 (2013).
36. Conroy, J. L., Cobb, K. M. & Noone, D. Comparison of precipitation isotope variability across the tropical Pacific in observations and SWING2 model simulations. *Journal of Geophysical Research:*

Atmospheres vol. 118 5867–5892 (2013).

37. Chiang, J. C. H. The Tropics in Paleoclimate. *Annual Review of Earth and Planetary Sciences* vol. 37 263–297 (2009).

38. Tierney, J. E., Smerdon, J. E., Anchukaitis, K. J. & Seager, R. Multidecadal variability in East African hydroclimate controlled by the Indian Ocean. *Nature* **493**, 389–392 (2013).

39. Timmermann, A. A Nonlinear Mechanism for Decadal El NiñO Amplitude Changes. *Geophysical Research Letters* vol. 29 (2002).

40. Timmermann, A. Decadal ENSO amplitude modulations: a nonlinear paradigm. *Global and Planetary Change* vol. 37 135–156 (2003).

41. Jin, F.-F. Strong El Niño events and nonlinear dynamical heating. *Geophysical Research Letters* vol. 30 (2003).

42. An, S.-I. & Jin, F.-F. Nonlinearity and Asymmetry of ENSO*. *Journal of Climate* vol. 17 2399–2412 (2004).

43. Liang, J., Yang, X.-Q. & Sun, D.-Z. The Effect of ENSO Events on the Tropical Pacific Mean Climate: Insights from an Analytical Model. *Journal of Climate* vol. 25 7590–7606 (2012).

44. Hayashi, M. & Jin, F. Subsurface Nonlinear Dynamical Heating and ENSO Asymmetry. *Geophysical Research Letters* vol. 44 (2017).

45. Karnauskas, K. B., Smerdon, J. E., Seager, R. & González-Rouco, J. F. A Pacific Centennial Oscillation Predicted by Coupled GCMs*. *Journal of Climate* vol. 25 5943–5961 (2012).

46. Samanta, D. *et al.* Coupled Model Biases Breed Spurious Low-Frequency Variability in the Tropical Pacific Ocean. *Geophysical Research Letters* vol. 45 (2018).

47. Koutavas, A. & Joanides, S. El Niño-Southern Oscillation extrema in the Holocene and Last Glacial Maximum. *Paleoceanography* vol. 27 (2012).

48. Rustic, G. T., Koutavas, A., Marchitto, T. M. & Linsley, B. K. Dynamical excitation of the tropical Pacific Ocean and ENSO variability by Little Ice Age cooling. *Science* **350**, 1537–1541 (2015).

49. Sadekov, A. Y. *et al.* Palaeoclimate reconstructions reveal a strong link between El Niño-Southern Oscillation and Tropical Pacific mean state. *Nature Communications* vol. 4 (2013).

50. Sigl, M. *et al.* Timing and climate forcing of volcanic eruptions for the past 2,500 years. *Nature* **523**, 543–549 (2015).

585 51. Tung, K.-K. & Zhou, J. The Pacific's Response to Surface Heating in 130 Yr of SST: La Niña–like or
586 El Niño–like? *Journal of the Atmospheric Sciences* vol. 67 2649–2657 (2010).
587 52. Adams, J. B., Brad Adams, J., Mann, M. E. & Ammann, C. M. Proxy evidence for an El Niño-like
588 response to volcanic forcing. *Nature* vol. 426 274–278 (2003).
589 53. McGregor, S., Timmermann, A. & Timm, O. A unified proxy for ENSO and PDO variability since
590 1650. *Climate of the Past* vol. 6 1–17 (2010).
591 54. Li, J. *et al.* El Niño modulations over the past seven centuries. *Nature Climate Change* vol. 3 822–826
592 (2013).
593 55. Khodri, M. *et al.* Tropical explosive volcanic eruptions can trigger El Niño by cooling tropical Africa.
594 *Nature Communications* vol. 8 (2017).
595 56. Mann, M. E., Cane, M. A., Zebiak, S. E. & Clement, A. Volcanic and Solar Forcing of the Tropical
596 Pacific over the Past 1000 Years. *Journal of Climate* vol. 18 447–456 (2005).
597 57. Ohba, M., Shiogama, H., Yokohata, T. & Watanabe, M. Impact of Strong Tropical Volcanic
598 Eruptions on ENSO Simulated in a Coupled GCM. *Journal of Climate* vol. 26 5169–5182 (2013).
599 58. Maher, N., McGregor, S., England, M. H. & Gupta, A. S. Effects of volcanism on tropical variability.
600 *Geophysical Research Letters* vol. 42 6024–6033 (2015).
601 59. Stevenson, S., Otto-Bliesner, B., Fasullo, J. & Brady, E. 'El Niño Like' Hydroclimate Responses to
602 Last Millennium Volcanic Eruptions. *Journal of Climate* vol. 29 2907–2921 (2016).
603 60. Predybaylo, E., Stenchikov, G. L., Wittenberg, A. T. & Zeng, F. Impacts of a Pinatubo-size volcanic
604 eruption on ENSO. *Journal of Geophysical Research: Atmospheres* vol. 122 925–947 (2017).
605 61. Liu, F. *et al.* Divergent El Niño responses to volcanic eruptions at different latitudes over the past
606 millennium. *Climate Dynamics* vol. 50 3799–3812 (2018).
607 62. Zuo, M., Man, W., Zhou, T. & Guo, Z. Different Impacts of Northern, Tropical, and Southern
608 Volcanic Eruptions on the Tropical Pacific SST in the Last Millennium. *Journal of Climate* vol. 31
609 6729–6744 (2018).
610 63. Sigl, M. *et al.* Insights from Antarctica on volcanic forcing during the Common Era. *Nature Climate*
611 *Change* vol. 4 693–697 (2014).
612 64. Liu, J. *et al.* Centennial Variations of the Global Monsoon Precipitation in the Last Millennium:
613 Results from ECHO-G Model. *Journal of Climate* vol. 22 2356–2371 (2009).

65. Coats, S. & Karnauskas, K. B. Are simulated and observed twentieth century tropical pacific sea surface temperature trends significant relative to internal variability?: Tropical pacific SST trends in CGCMs. *Geophys. Res. Lett.* **44**, 9928–9937 (2017).
66. Delfin, F. G., Panem, C. C. & Defant, M. J. Eruptive history and petrochemistry of the Bulusan volcanic complex: Implications for the hydrothermal system and volcanic hazards of Mt. Bulusan, Philippines. *Geothermics* vol. 22 417–434 (1993).
67. Blaauw, M. & Andrés Christen, J. Flexible paleoclimate age-depth models using an autoregressive gamma process. *Bayesian Analysis* vol. 6 457–474 (2011).
68. M. Blaauw, J. A. Christen, Bacon, 352. <http://www.chrono.qub.ac.uk/blaauw/bacon.html&gt. (2015).
69. Reimer, P. J. *et al.* IntCal13 and Marine13 Radiocarbon Age Calibration Curves 0–50,000 Years cal BP. *Radiocarbon* vol. 55 1869–1887 (2013).
70. Rach, O., Hadeen, X. & Sachse, D. An automated solid phase extraction procedure for lipid biomarker purification and stable isotope analysis. *Organic Geochemistry* vol. 142 103995 (2020).
71. Bennett, K. D. & Willis, K. J. Pollen. *Tracking Environmental Change Using Lake Sediments* 5–32 doi:10.1007/0-306-47668-1_2.
72. Yoshimura, K. Stable Water Isotopes in Climatology, Meteorology, and Hydrology: A Review. *Journal of the Meteorological Society of Japan. Ser. II* vol. 93 513–533 (2015).
73. Kanamitsu, M. *et al.* NCEP–DOE AMIP-II Reanalysis (R-2). *Bulletin of the American Meteorological Society* vol. 83 1631–1643 (2002).
74. Yoshimura, K., Kanamitsu, M., Noone, D. & Oki, T. Historical isotope simulation using Reanalysis atmospheric data. *Journal of Geophysical Research* vol. 113 (2008).
75. J. M. Wallace, T. P. Mitchell, A. K.-H. Lau, Legates/MSU precipitation climatology, 342. <http://http://research.jisao.washington.edu/legates_msu/> (1995).
76. PHILGIS, Philippine GIS Datasets,. <http://philgis.org/gis-data> (2017).
77. Quantum GIS Development Team, Quantum GIS Geographic Information System, 345. Open Source Geospatial Foundation Project,. <http://qgis.osgeo.org> (2016).
78. SIO, NOAA, U.S.Navy, NGA, 348 GEBCO, Image Landsat, Data LDEO-Colombia, NSF. Google Earth Map [7.1.5.1557. Bulusan Lake, Philippines. 12° 26’ 07.68” N, 123° 347 48’ 29.53” E, Eye alt

643 2683.13 km]. (2016).
644 79. R Core Team, R: A language and environment for statistical computing, 354. <http://www.R-
645 project.org/> (Foundation for Statistical Computing, Vienna, Austria, 355 2013).
646 80. Croudace, I. W. & Guy Rothwell, R. ItraxPlot: An Intuitive Flexible Program for Rapidly Visualising
647 Itrax Data. *Micro-XRF Studies of Sediment Cores* 613–624 (2015) doi:10.1007/978-94-017-9849-
648 5_26.
649 81. Wickham, H. *ggplot2: Elegant Graphics for Data Analysis*. (Springer Science & Business Media,
650 2009).

Supplementary Information for

Abrupt shift to El Niño-like mean state conditions in the tropical Pacific during the Little Ice Age

Ana Prohaska*, Alistair W.R. Seddon, Bernd Meese, Katherine J. Willis, John C. H. Chiang, Dirk Sachse

*Corresponding author. Email: ap989@cam.ac.uk

This PDF file includes:

Supplementary Text
Figs. S1 to S10
Tables S1 to S3

Supplementary Text

1. Physical and chemical characterisation of Bulusan cores

Laminations in the Bulusan sediments were mapped using a combination of optical and radiograph images taken with the Itrax Core Scanner[1] at 0.2 mm resolution at the University of Aarhus in September 2013. These data were used to link the 1 m segments of the two sedimentary sequences into a single composite core with undisturbed sediments (Fig. 2d). Though Bulusan sediments are finely laminated throughout the sequence, given the low frequency, uneven thickness, and widely varying colour of these formations, they are unlikely to represent varves (i.e., annual laminations). While the origin of the Bulusan laminations remains uncertain, likely candidates include droughts, storms, seasonal changes in algal communities and any combination of these. There is also a possibility that some laminations reflect past El Niño events (e.g., extreme drought conditions). However, more detailed investigations are required to confirm this possibility, and this particular inquiry is beyond the scope of our study. Therefore, the principal purpose of the lamination analysis is to confirm the absence of any local depositional events and sediment slumping that may have influenced the Bulusan record.

Magnetic susceptibility measurements were taken on intact Bulusan cores using the Barrington MS2 Magnetic Susceptibility System made of a magnetic susceptibility meter coupled with a core logging sensor at 2 cm spatial resolution and 11s SI (9s CGS) measurement period. Arithmetic mean of magnetic susceptibility values was calculated over 4 cm long slices to align the data with the sample resolution of $n\mathrm{C}_{27\text{-}31}$ alkanes. The magnetic susceptibility values are relatively low throughout the Bulusan sequence apart from four sharp peaks which correspond to <1 cm thick tephra layers (Fig. S2). These results indicate consistently low soil erosion rates into the Bulusan Lake which is to be expected given the thick forest cover that surrounds it. The four tephra layers have likely been created during past volcanic eruptions of the nearby Mount Bulusan volcano, though other volcanoes in the region such as the very active Mount Mayon represent another potential source of the tephra material deposited in the Bulusan sediments.

2. Age-Depth Model assessment

The analysis of the chronological uncertainty of the age-depth model for the $n\mathrm{C}_{29}$ alkane δD record shows that the model is well constrained, particularly around the marked increase in the $\delta\mathrm{D}_{wax}$ values (Fig. S10). This is due to a relatively high density of radiocarbon dates generated for the Bulusan record (Table S1). The two seemingly reversed radiocarbon dates have little bearing on the age-depth model reliability. The first of these - SUERC-64003 - is most likely due to its $\delta^{13}\mathrm{C}$ value being an estimated value because there was insufficient amount of material for an

independent $\delta^{13}C$ measurement. The age-depth model corrected for this by excluding this particular date as an outlier. The other potentially reversed date – SUERC-64006 - comes from the lower portion of the core, far away from its dry period section and, consequently, it's influence on the timing of the discussed change in δD_{wax} values ~AD 1630 is negligible. Lastly, the photographic and radiographic profile of the Bulusan sedimentary sequence, presented in Fig. 2d, as well as the magnetic susceptibility record (Fig. S2), show undisturbed laminations throughout the core sequence, excluding the possibility of sediment slumping, the presence of depositional events (e.g., floods) or significant changes in the sedimentation rate. Since the lake is 12 meters deep and no prior coring activities have taken place, it is highly unlikely that the top sediment layer was disturbed or removed, and thus the top of the sediment core has been assigned the year when the core was collected, i.e., 2013. Overall, this information demonstrates high reliability of the age-depth model.

3. Influx rates of *n*-alkanes

Influx rates of *n*-alkanes, calculated as weight of *n*-alkanes deposited in a g of dry sediment in a year (g g_{sed}^{-1} yr^{-1}), ranged widely between different alkanes, with nC_{27-31} being the most dominant among them. While the nC_{29} and nC_{31} alkanes exhibit similar patterns in abundance variability along the sequence, the nC_{27} alkane showed a dissimilar pattern, indicating a different origin of nC_{27} in relation to nC_{29} and nC_{31} (Fig. S3a).

The high bi-decadal variability of δD_{wax} values (up to ±10 ‰) suggests rapid transfer of leaf waxes into the lake sediments as opposed to the scenario of substantial residence time (e.g., in soils) which would result in signal dampening.

4. Average chain length of *n*-alkanes

Average chain length of *n*-alkanes (ACL), calculated as $(25*A_{25} + 27*A_{27} + 29*A_{29} + 31*A_{31} + 33*A_{33}) / (A_{25} + A_{27} + A_{29} + A_{31} + A_{33})$, has remained around 30 throughout the record, except for a slight drop in the values to 28-29 over the last 200 years (Fig S3b). Human activities such as logging and harvesting of certain tree species (e.g., rattan) have been recorded in the area during this time[2], and the associated changes in the forest composition may have been the underlying cause to this drop in the ACL values.

5. Correlation between *n*-alkane records

The Pearson product-moment correlation coefficient was used to measure dependence between pairs of nC_{29-31} alkanes, and the significance of this dependence was evaluated with Welch's t-test (p-value set to 0.05, equal variance not required[3]). Prior to this calculation, we accounted for

temporal autocorrelation in the alkane records by first calculating the time between independent values (or the time to obtain a new degree of freedom, τ) and then used τ values to calculate the effective sample size (i.e., the effective number of independence values, n_{eff}), as outlined in ref.[4], with autocorrelation value set at the lag of 1 data point for both records.

Results show that the δD values of the three abundant terrestrial lipid biomarkers in the Bulusan core, nC$_{27-31}$, are highly correlated (Fig. S4). The relationship between nC$_{27}$ and nC$_{29}$ had the highest correlation coefficient (~ 0.81), followed by the coefficients for the nC$_{27}$ and nC$_{31}$ and the nC$_{29}$ and nC$_{31}$ (~ 0.69). P-values were highly significant for all three relationships (i.e., $<10^{-6}$). The results confirm a common origin of these three *n*-alkanes.

6. Source variation of *n*-alkanes

While previous studies have suggested that grasses and trees both can be important contributors of nC$_{29}$ and nC$_{31}$ alkanes[5,6], the pollen record from the Bulusan site (Fig. 3) shows the dominance of arboreal and shrub taxa over grasses throughout the Bulusan record, and thus suggests that trees and shrubs were the main source of C$_{27-31}$ alkanes in the Bulusan record. A recent study by Feakins et al.[5], looking at the production of leaf wax *n*-alkanes across a tropical rain forest elevation transect and showing that tropical trees are dominated by both nC$_{29}$ and nC$_{31}$ alkanes (followed by nC$_{27}$ alkane), provides further support to this interpretation. While the changes in nC$_{27}$/ nC$_{29}$ and nC$_{27}$/ nC$_{31}$ ratio and the ACL index values in the Bulusan record (Fig. S3) indicate somewhat variable alkane sources, these are more likely to have been caused by the changes in the relative abundance of different tree and shrub taxa over time (Fig. S5), rather than brought about by the changes in the trees and shrub/ grasses ratio. Since the pollen data from this site indicate a relatively stable ratio of grasses to other terrestrial plant taxa, it is unlikely that the recorded changes in the C$_{27-29}$ ratio in the Bulusan record have translated into changes in the C3/C4 pathways and exerted a major influence on δD of alkanes.

Transport of alkanes to the lake was most likely a combination of direct leaf input into the lake (there is high incidence of tropical storms at the site, often leaving a blanket of leaves on lake surface (Bulusan Natural Park managers, pers. comm.) and erosion (high precipitation levels throughout the year (Fig. S1a)). Given the closed nature of the Bulusan lake basin (no known inlets/outlets), we expect that pollen transport has been mostly eolian. Previous studies on pollen transport in tropical forest environments[7,8] showed that pollen gives a more local signal (distance in 10s m) in these environments, which closely corresponds to the generally local nature of alkane sources in small catchment lakes such as Bulusan, and makes the two records readily comparable.

7. Detection of regime shifts

The Sequential T-test Analysis of Regime-Shift algorithm (STARS)[9,10] was used to detect significant changes (p-value set to <0.05) in the mean of δD values of the nC$_{27-29}$ alkanes. To address uneven spacing of the samples, the time series was sorted into the smallest bin size that still generated a continuous record (i.e., 22 years), and then standardized by the mean and standard deviation. Since the STARS algorithm assumes normality and does not explicitly account for autocorrelation, the time series was transformed to normal distribution using Box Cox transformation and passed through a white-noise filter using the ordinary least-squares method outlined in Rodionov[10] using a version of the STARS algorithm coded in R[11,12].

The STARS algorithm detected two significant changes in the mean of δD values of the nC$_{27-29}$ alkane records (Tables S3-5, Fig. S6). The first shift was towards lower δD values at ~AD 1630 and was followed by a shift to higher δD values at ~AD 1900. These results confirm significantly lower precipitation at Bulusan Lake during the latter half of the LIA (~AD 1630–1900), compared to the rest of the examined record.

8. Annual rainfall amount and δD values in the Bulusan area from instrumental measurements

To complement the analysis of CRU TSv4 rainfall and δD_{pw} in isoGSM2, we examine the variability in modern monthly precipitation amount and modern precipitation δD (δD_{precip}) values for the wider Bulusan area using instrumental measurements from seven GNIP sites near Bulusan spanning the period from 1990-1998: Balasbas (N 13°6'0", E 123°54'0"), Bonga station (N 13°1'48", E 123°55'12"), Botong (N 13°3'0.00", E 123°58'12"), Cawayan (N 13°1'48.00", E 123°56'24"), Guinlajon (N 13°0'36", E 123°57'36"), Inang (N 13°4'12", E 123°54'36") and Palayang (N 13°3'36", E 123°55'48")[13] (Fig S9). Note that while GNIP station data more directly addresses precipitation and δD_{precip} characteristics for the Bulusan area, the data is also quite limited and suffers from missing data, making it unsuitable for analyzing interannual variability.

9. Relationship between δD of precipitable water and δD of precipitation

We evaluated the relationship between δD of precipitable water from isoGSM2 output and δD of precipitation from the GNIP sites close to Bulusan, along with typhoons and heavy storms, using Generalised Linear Least Squares (GLS), with GNIP δD as the response variable and isoGSM2 δD values as the explanatory variable (Fig. S7). GLS is an extended linear fixed-effects model in which errors are permitted to be correlated and/ or have unequal variance[14]. Several GLS models were applied in R version 3.5.2.[11] using the nlme 3.1-128 package[15] with different combinations

of temporal correlation and variance structures imposed on the error components to allow unequal variance of the errors[16]. Errors were specified to follow an autoregressive-moving-average (ARMA) process and variance structure was defined with the explanatory variable as a variance covariate. The validity of individual models was then evaluated using standard diagnostic tests[16]. The best fitting model with satisfying diagnostics was selected based on the lowest Akaike Information Criterion (AIC) coefficients with a simpler model selected whenever the difference in AIC coefficients between two models was smaller than 2[17]. Models were considered significant at the 95% level of confidence. Positive and negative slopes are indicated as (+) or (−), respectively. Data were sourced from GNIP[13] and isoGSM2[18], plotted with *ggplot2* package[19] in R version 3.5.2.[11].

The results confirm that δD of precipitable water, given by isoGSM2, closely corresponds to δD of precipitation, provided by GNIP data, in the Bulusan area, especially when the effect of typhoons and heavy storms is included (Fig. S7, Table S3). Specifically, GLS models show a positive effect of precipitable water δD (isoGSM2) (and negative effect of typhoons/ storms) on rainfall δD (GNIP data).

These results allow us to directly relate the observed pattern of δD precipitable water in isoGSM2 to changes in δD of precipitation for the Bulusan area and estimate the effect of El Niño (and La Niña) on precipitation-weighted δD. For example, in August, the precipitation δD from the GNIP sites is around -50 per mil, so if we take an offset of +127 per mil to the δD of precipitable water to estimate the δD of rainfall, we get a precipitation weighted δD of -18.2 per mil for El Niño rainfall, -23.6 per mil for La Niña rainfall, and -22.7 per mil for neutral rainfall. According to these calculations, El Niño rainfall is isotopically heavier by about +5 per mil than La Niña. Therefore, while there is less winter rainfall for El Niño years, the fact that El Niño precipitable water δD is heavier overrides the effect of less winter rainfall.

10. The influence of solar irradiance on hydrological conditions at Bulusan site

We have compared a solar irradiance record[20–22] with the nC$_{29}$ alkane record from the Bulusan Lake to examine the influence of irradiance variability on the precipitation conditions at the site over the last 1,400 years. The period of low solar irradiance between ~AD 1400-1750 has been linked to ITCZ migration and thus, notable changes in the precipitation dynamics of tropical Pacific records in response to this time interval are likely to be caused by changes in the ITCZ position or its latitudinal extent. However, the period of increased δD_{wax} values in the Bulusan record (i.e., ~AD 1630-1900) has a poor overlap with this period of low solar irradiance. This holds true even after the uncertainty of the Bulusan age-depth model is considered (i.e., mean

95% confidence range is 101.2 years, min. 41 years at 0 cm, max. 154 years at 299 cm) (Fig. S10), suggesting that this abrupt precipitation reduction at Bulusan Lake is unlikely to have been driven by irradiance variability/ ITCZ changes.

Supplementary Figures and Tables

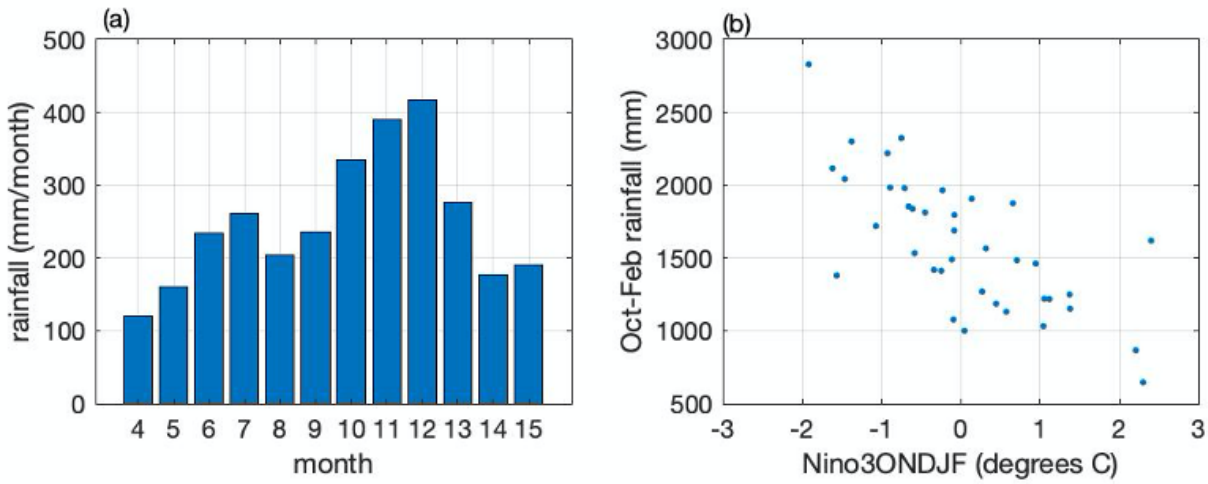

Fig. S1. (a) Monthly mean precipitation at Bulusan, using the CRU TSv4 gridpoint closest to Bulusan lake (N 12°45', E 124°15'). The climatology is calculated from 1979-2017, and the month covers April through the following March. The onset of the Western North Pacific monsoon is apparent in the rainfall peak around June-July, but the main rainfall season is in winter. The summer months of June-September contribute ~31% of the total annual rainfall, whereas the winter months of October-January contribute ~47%. **(b) Relationship between wintertime rainfall over Bulusan with ENSO.** Nino3.4 averaged over Oct-Feb (x-axis) plotted against Bulusan rainfall summed over the Oct-Feb period. The correlation coefficient between the two is -0.72 ($p<0.001$).

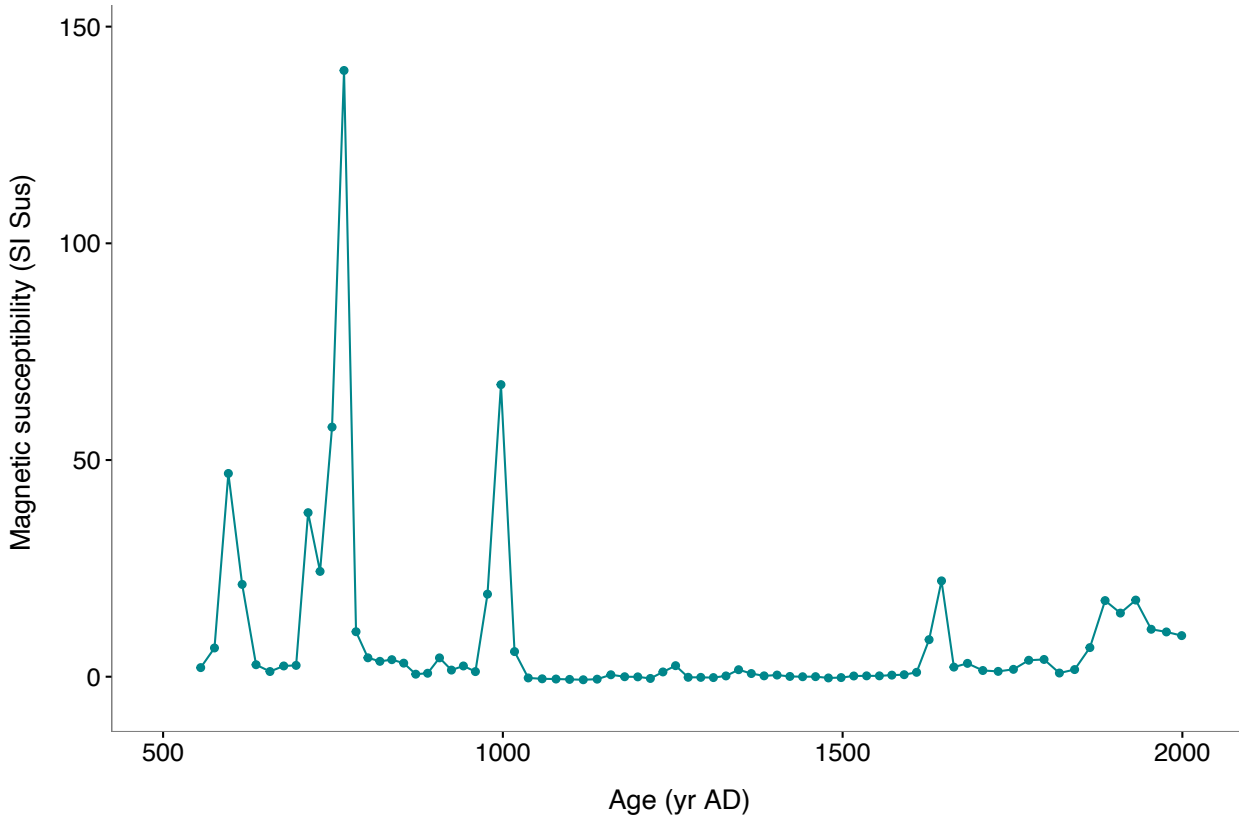

187

188 **Fig. S2. Magnetic susceptibility measurements from the Bulusan sedimentary core.** The four
189 sharp peaks in measurement values correspond to <1 cm thick tephra layers. Data plotted with
190 *ggplot2* package [19] in R version 3.2.4[11].

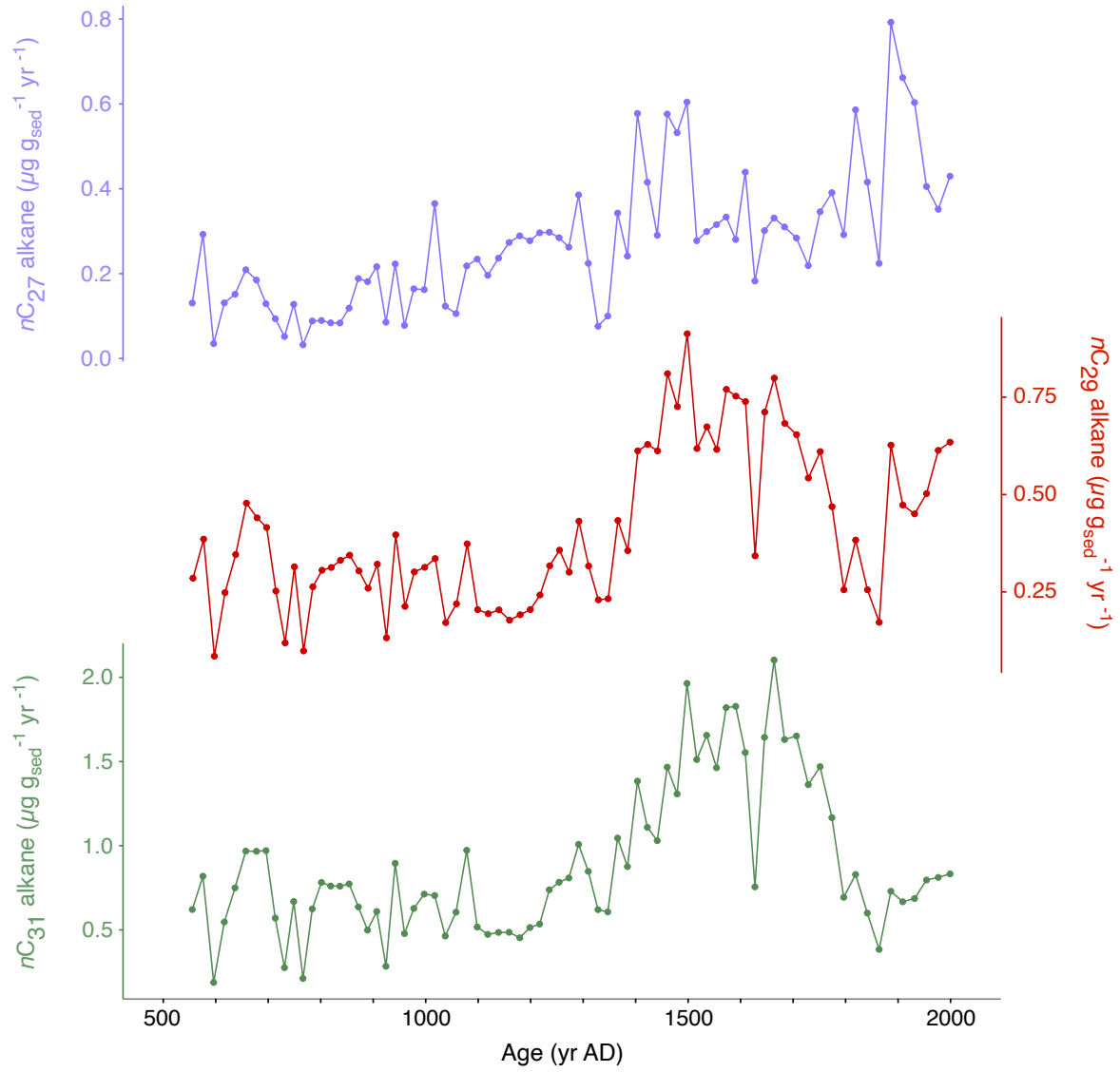

(a)

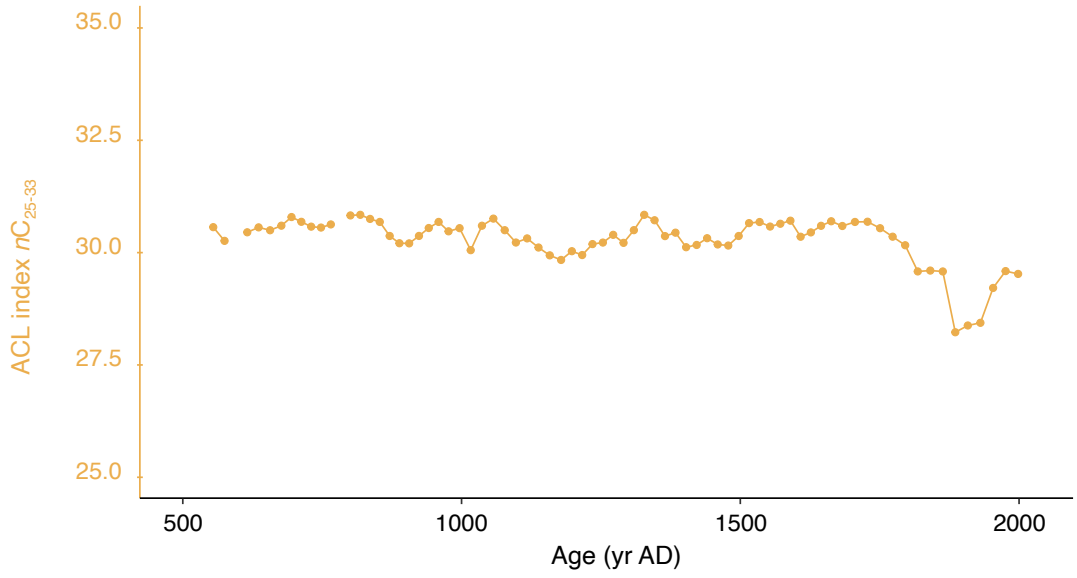

(b)

Fig. S3. (a) Influx rates of *n*C$_{27-31}$ alkanes in the Bulusan sedimentary sequence in µg per g of sediment (dry weight) per year. (b) Average chain length (ACL) of *n*C$_{25-33}$ alkanes in the Bulusan record. Data plotted with *ggplot2* package[19] in R version 3.2.4[11].

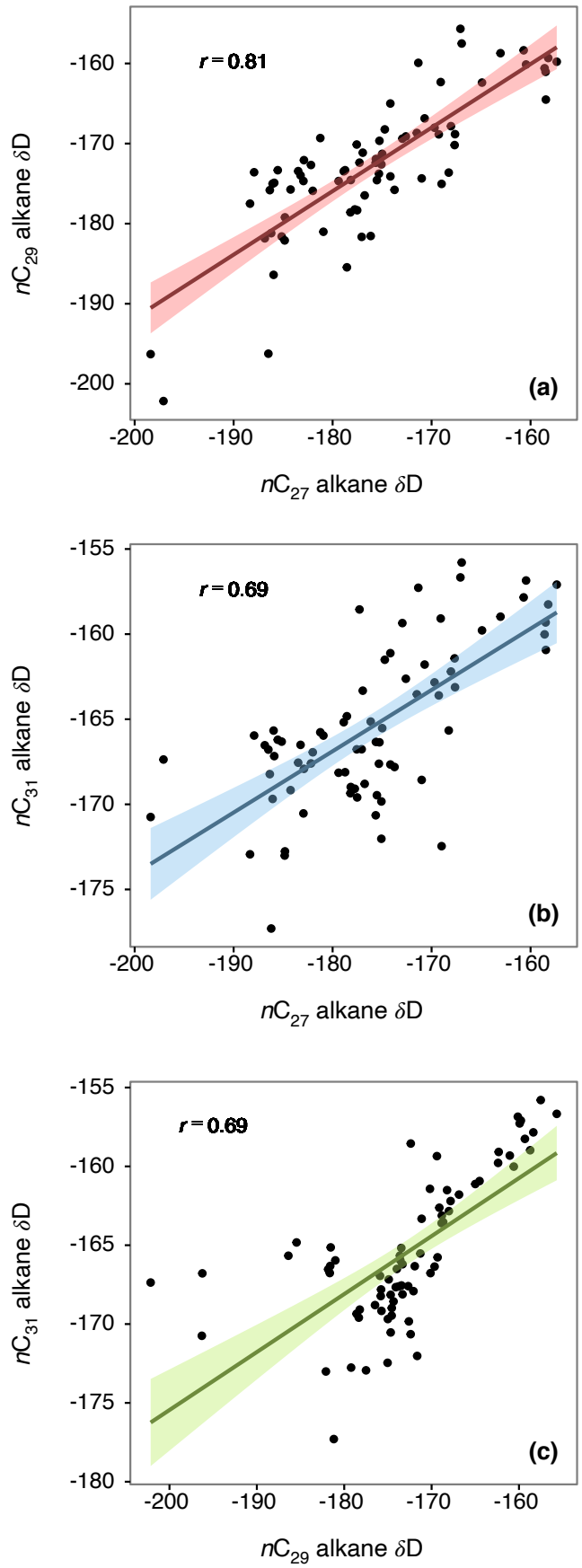

196

197 **Fig. S4. Correlation between the δD values of *n*-alkanes from the Bulusan sedimentary core.**
198 **(A)** nC_{27} and nC_{29} alkanes (p-value = 4.9×10^{-12}), **(B)** nC_{27} and nC_{31} alkanes (p-value = 1.8×10^{-7}), and
199 **(C)** nC_{29} and nC_{31} alkanes (p-value = 2.1×10^{-7}). Data plotted with *ggplot2* package[19] in R version
200 3.2.4[11].

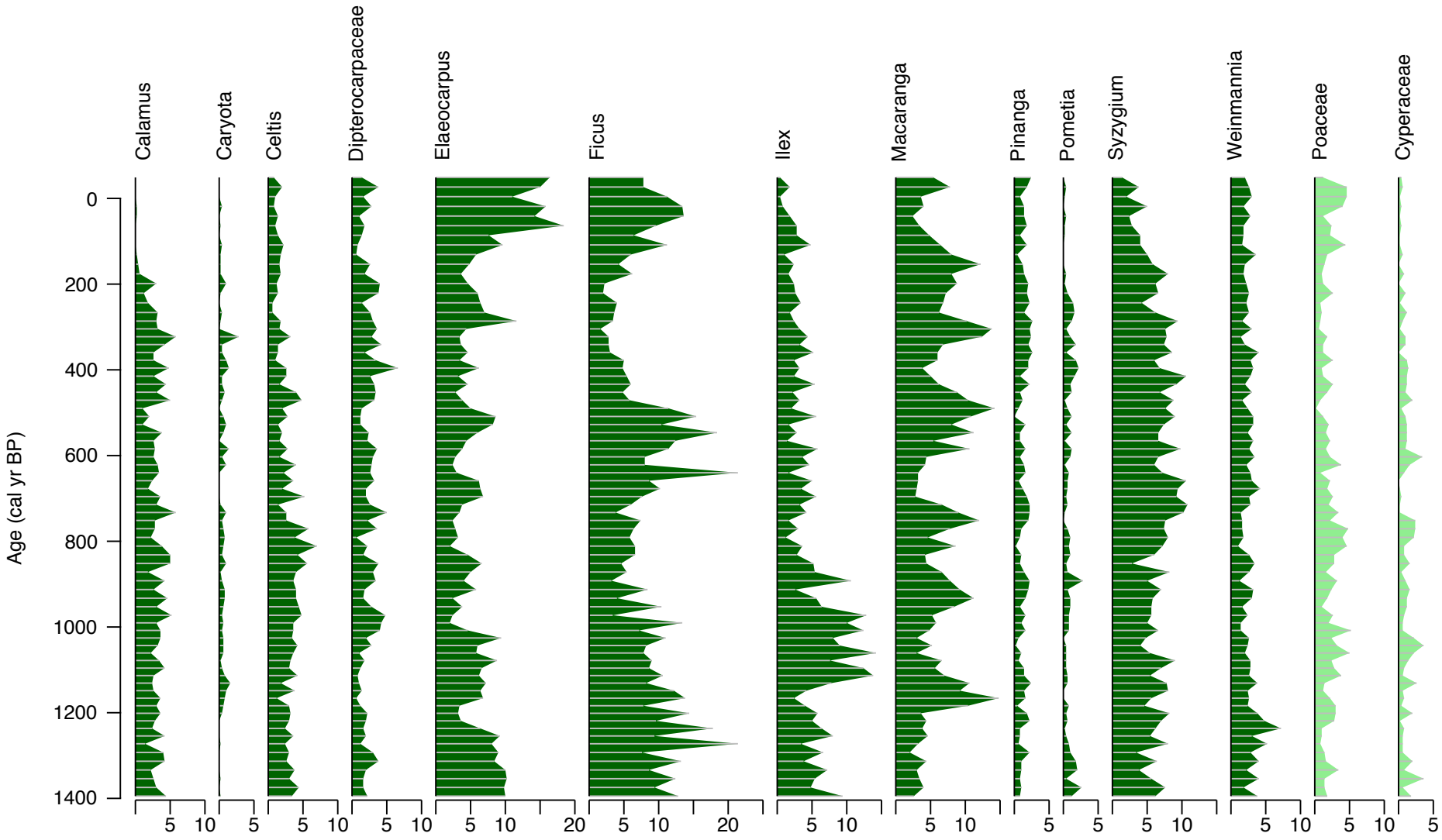

Fig. S5. Pollen abundance of individual taxa (family/ genus) expressed as a percentage of the total terrestrial pollen grains (%, x-axis). The diagram was generated using the *rioja* package[23] in the R version 3.2.4[11].

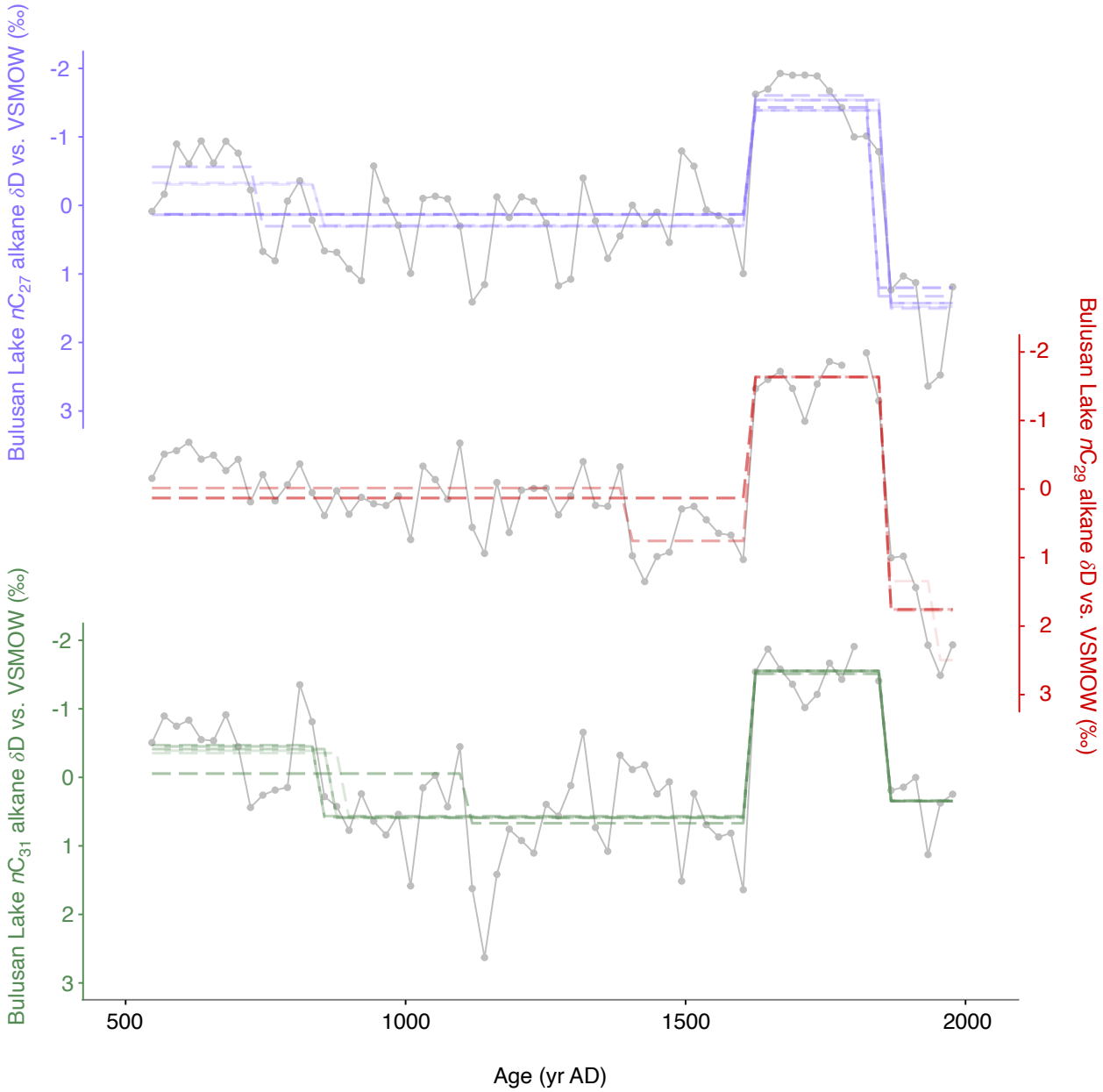

Fig. S6. Significant changes in the mean of δD values of *n*C$_{29}$ alkane record from the Bulusan sequence, as detected with the STARS algorithm. The grey line depicts δD values of *n*C$_{29}$ alkane after Box Cox transformation and pre-whitening. Overlaying blue lines depict the sequential sample mean of *n*C$_{29}$ δD record for incremental time windows size from 5 to 15 data points (~100-300 yrs). Significance of the change in the sample mean is set to p-value <0.05. Data plotted with *ggplot2* package[19] in R version 3.2.4[11].

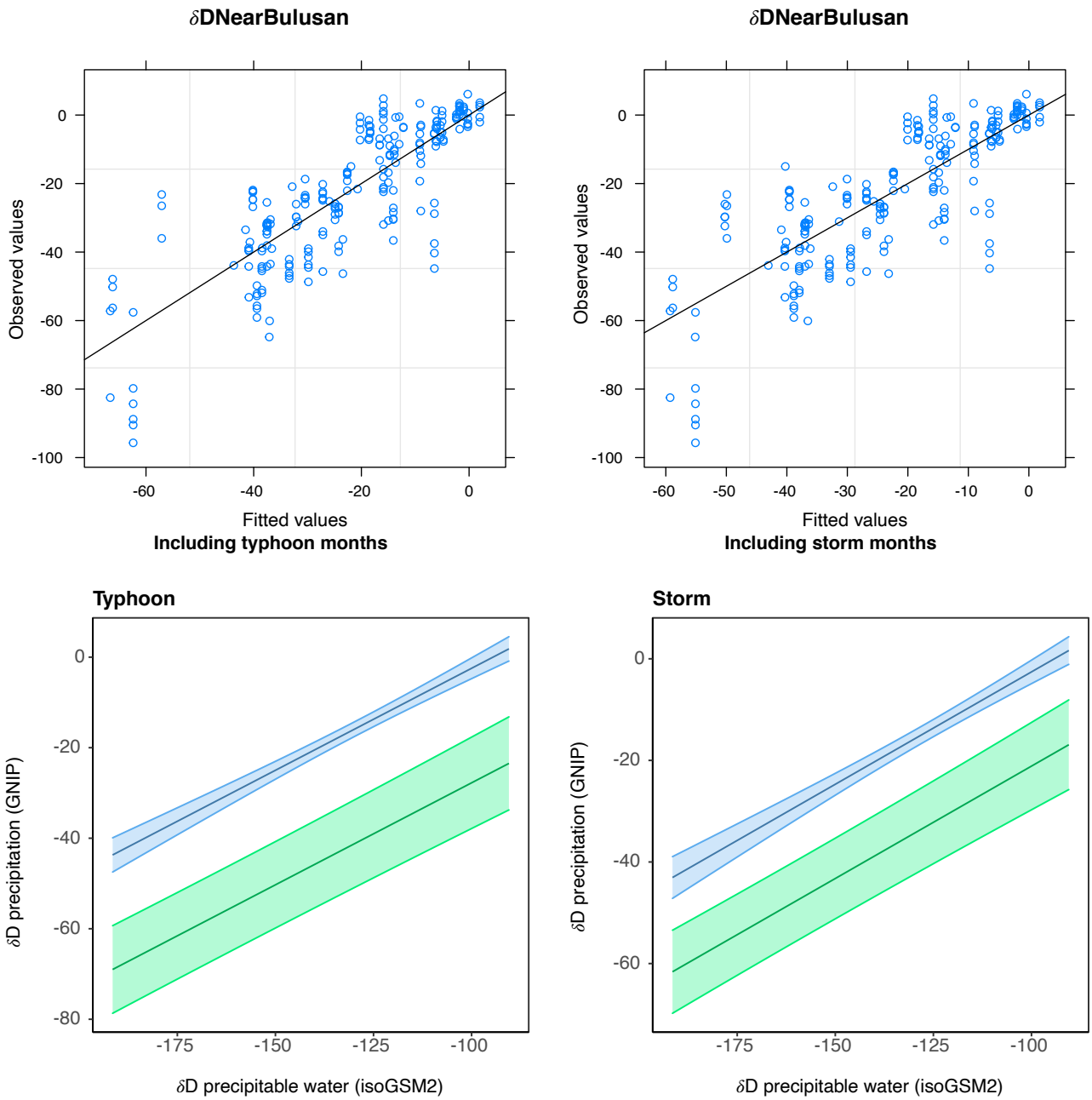

211

212 **Fig. S7. Best fitted GLS models of the relationship between δD of precipitable water from**
213 **isoGSM2 output and δD of precipitation from the GNIP sites close to Bulusan, along with**
214 **typhoons and heavy storms.** Upper panel shows model fit, and the lower panel shows model
215 predicted relationship between the variables (blue curve indicates relationship under regular
216 conditions, and green relationship under typhoon or storm conditions). Data from GNIP[13] and
217 isoGSM2[18], plotted with *ggplot2* package[19] in R version 3.5.2.[11].

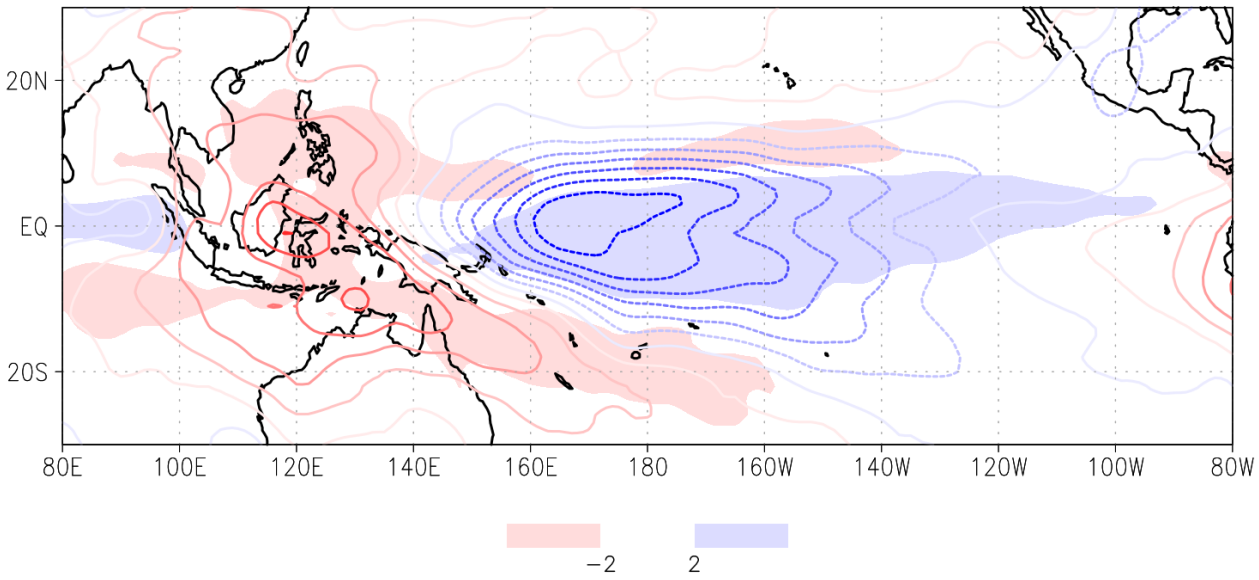

Fig. S8. Change to δD_{pw} and rainfall associated with El Niño. Shown are the El Niño minus La Niña composites of October-February averaged δD of precipitable water (δD_{pw}) (contour interval 5 per mil, blue dashed lines are negative) and precipitation (shaded; red shading is < -2 mm/d, and blue shading is > 2mm/d). Note in particular the enriched δD_{pw} over the western tropical Pacific tied to a decrease in rainfall over the region.

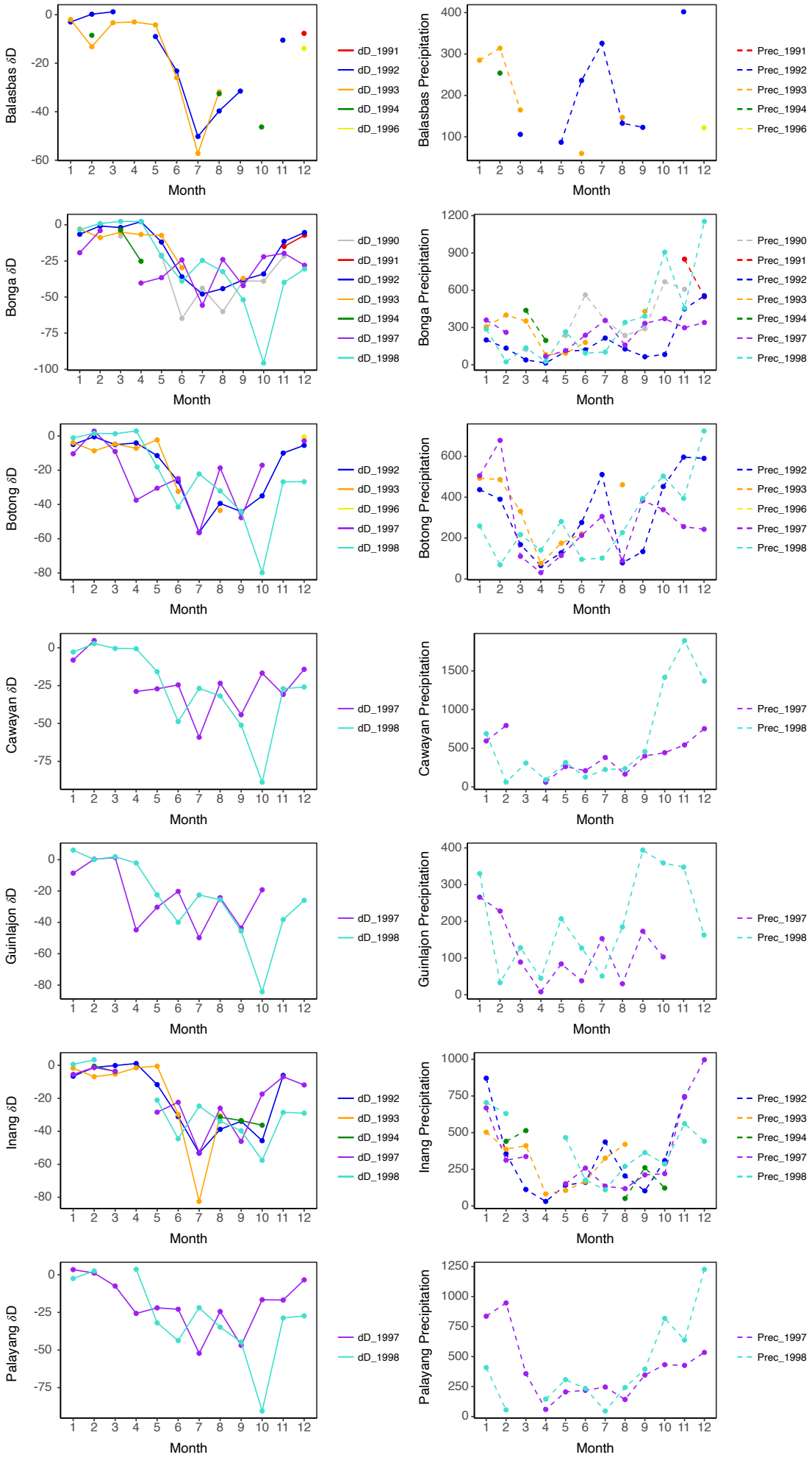
Balasbas δD
Month
dD_1991
dD_1992
dD_1993
dD_1994
dD_1996
Balasbas Precipitation
Prec_1991
Prec_1992
Prec_1993
Prec_1994
Prec_1996
Bonga δD
dD_1990
dD_1991
dD_1992
dD_1993
dD_1994
dD_1997
dD_1998
Bonga Precipitation
Prec_1990
Prec_1991
Prec_1992
Prec_1993
Prec_1994
Prec_1997
Prec_1998
Botong δD
dD_1992
dD_1993
dD_1996
dD_1997
dD_1998
Botong Precipitation
Prec_1992
Prec_1993
Prec_1996
Prec_1997
Prec_1998
Cawayan δD
dD_1997
dD_1998
Cawayan Precipitation
Prec_1997
Prec_1998
Guinlajon δD
Guinlajon Precipitation
Inang δD
Inang Precipitation
Palayang δD
Palayang Precipitation

Fig. S9. Seasonality of rainfall in the Bulusan area. Average monthly values spanning the period from 1990-1998 (years not continuous for all sites). Precipitation δD and precipitation amount values measured at the GNIP sites near the Bulusan site[13]. Data plotted with *ggplot2* package[19] in R version 3.5.2.[11].

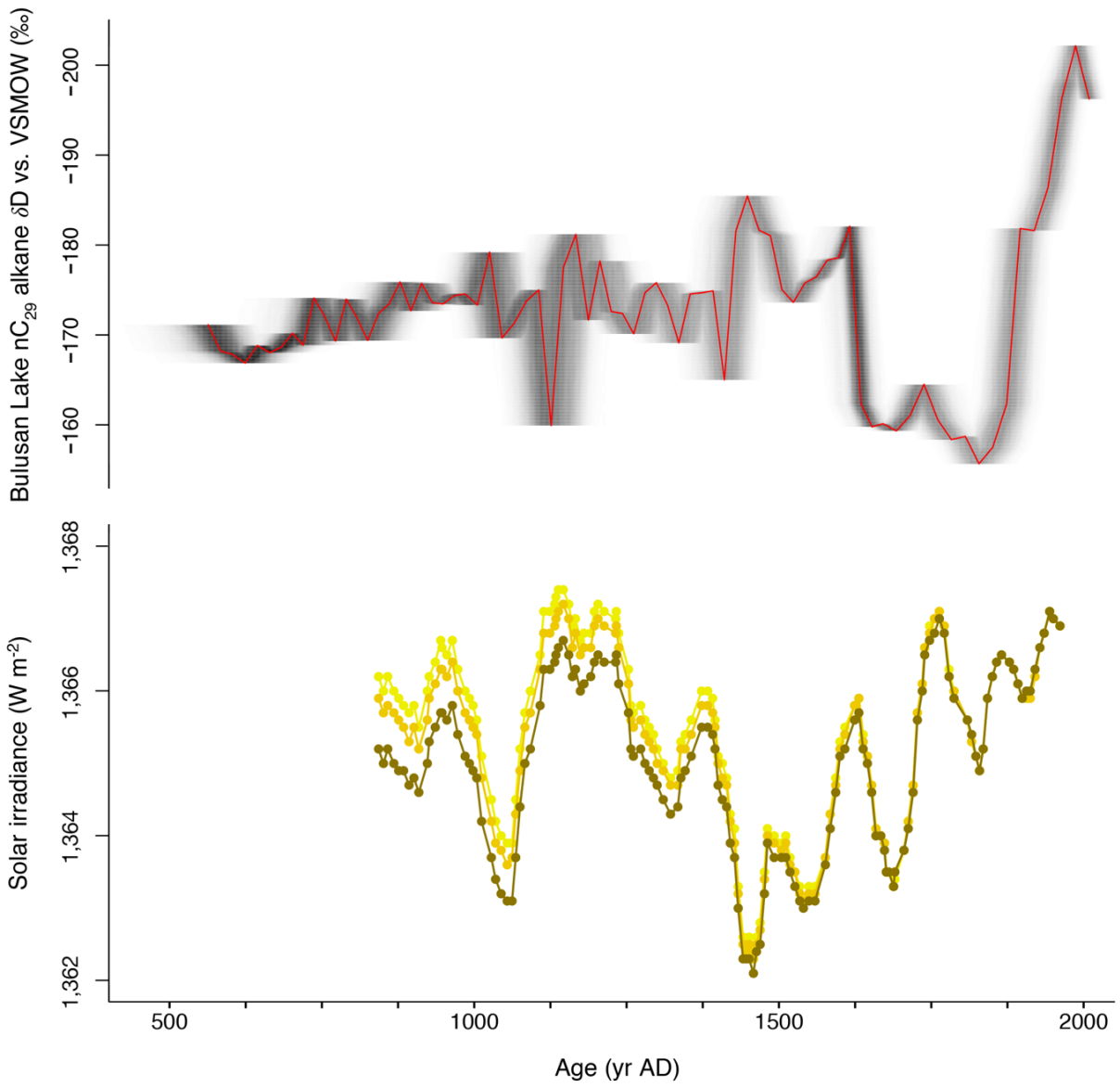

Fig. S10. Comparison of the *n*C$_{29}$ alkane δD record from the Bulusan sedimentary sequence and three different calibrations of the solar irradiance variability record, TSI (Wm^{-2})[20–22]. The *n*C$_{29}$ alkane δD record includes the chronological uncertainty of the age-depth model[24] (grey shading, with darker grey indicating more likely calendar ages for specific proxy values). Data plotted with *Bacon 2.2*[25,26] *and ggplot2* package[19] in R version 3.2.4[11].

Lab ID	Sample Material	Core Depth (cm)	Radiocarbon Age (yr BP ± 1σ)	Carbon content (% by wt.)	δ13CVPD B‰ (± 0.1)
SUERC-64001	Terrestrial plant	59	240±35	55.2	-30.0
SUERC-64002	Terrestrial plant	69	293±37	57.7	-29.7
SUERC-64003	Terrestrial plant	74	450±37	38.9	-30.2*
SUERC-64005	Terrestrial plant	82	323±37	52.6	-28.7
SUERC-64004	Terrestrial plant	84	401±37	48.9	-31.6
SUERC-51111	Terrestrial plant	126	617±38	55.8	-29.9
SUERC-64006	Terrestrial plant	163	609±37	55.0	-31.2
SUERC-51112	Terrestrial plant	204.5	1146±35	46.3	-28.0
SUERC-64010	Terrestrial plant	272	1235±37	50.1	-29.2
SUERC-64011	Terrestrial plant	342.5	1629±37	58.0	-30.8

Table S1. AMS^{14}C dates of the Bulusan sedimentary sequence measured at the NERC Radiocarbon Facility, East Kilbride. * Estimated value, insufficient material for an independent 13C measurement.

Time window (no. data points)	Change Point 1 (AD 745 yr)	Change Point 2 (AD 855 yr)	Change Point 3 (AD 1625 yr)	Change Point 4 (AD 1845 yr)	Change Point 5 (AD 1867 yr)
5	/	* 3.42E-03	† 5.15E-11	/	*3.16E-05
6	/	/	† 3.73E-10	/	*3.16E-05
7	/	/	†3.73E-10	/	/*3.16E-05
8	*2.87E-05	/	†7.21E-12	*3.59E-04	/
9	*2.87E-05	/	†7.21E-12	*3.59E-04	/
10	/	/	†1.17E-10	*3.67E-04	/
11	/	/	†1.17E-10	*3.67E-04	/
12	/	/	†1.17E-10	*3.67E-04	/
13	/	*5.72E-03	†1.40E-10	/	*4.33E-05
14	/	/	†9.55E-10	/	*4.33E-05
15	/	/	†9.55E-10	/	*4.33E-05

Table S2a. The timing and p-values of the significant changes in the mean of δD values of the *n*C_{27} alkane in the Bulusan sequence identified by the STARS algorithm with incremental time window sizes. Increases and decreases in the sample mean are denoted by asterisk and obelisk, respectively.

Time window (no. data points)	Change Point 1 (AD 1405 yr)	Change Point 2 (AD 1625 yr)	Change Point 3 (AD 1867 yr)	Change Point 4 (AD 1945 yr)
5	*2.64E-05	†3.77E-12	*9.20E-04	*4.94E-02
6	/	†7.96E-12	*3.04E-05	/
7	/	†7.96E-12	*3.04E-05	/
8	/	†7.96E-12	*3.04E-05	/
9	*2.64E-05	†3.77E-12	*3.04E-05	/
10	*2.64E-05	†3.77E-12	*3.04E-05	/
11	*2.64E-05	†3.77E-12	*3.04E-05	/
12	/	†7.96E-12	*3.04E-05	/
13	/	†7.96E-12	*3.04E-05	/
14	/	†7.96E-12	*3.04E-05	/
15	/	†7.96E-12	*3.04E-05	/

Table S2b. The timing and p-values of the significant changes in the mean of δD values of the *n*C_{29} alkane in the Bulusan sequence identified by the STARS algorithm with incremental time window sizes. Increases and decreases in the sample mean are denoted by asterisk and obelisk, respectively.

Time window (no. data points)	Change Point 1 (AD 855 yr)	Change Point 2 (AD 877 yr)	Change Point 3 (AD 899 yr)	Change Point 4 (AD 1119 yr)	Change Point 5 (AD 1625 yr)	Change Point 6 (AD 1867 yr)
5	/	/	/	*8.39E-04	†1.61E-13	*5.38E-06
6	/	/	/	*8.39E-04	†1.61E-13	*5.38E-06
7	/	/	/	*8.39E-04	†1.61E-13	*5.38E-06
8	/	/	*5.52E-06	/	†1.30E-16	*5.38E-06
9	/	* 2.43E-06	/	/	†9.28E-17	*5.38E-06
10	/	*2.43E-06	/	/	†9.28E-17	*5.38E-06
11	*1.54E-06	/	/	/	†7.74E-17	*5.38E-06
12	*1.54E-06	/	/	/	†7.74E-17	*5.38E-06
13	*7.52E-06	/	/	/	†1.55E-16	*6.39E-06
14	*7.52E-06	/	/	/	†1.55E-16	*6.39E-06
15	/	*1.15E-05	/	/	†1.88E-16	*6.39E-06

Table S2c. The timing and p-values of the significant changes in the mean of δD values of the *n*C_{31} alkane in the Bulusan sequence identified by the STARS algorithm with incremental time window sizes. Increases and decreases in the sample mean are denoted by asterisk and obelisk, respectively.

Storms/ Typhoon	*Only typhoons included*	*All heavy storms included*
Model Structure	δDNearBulusan ~ δDISOGSM2 + typhoons	δDNearBulusan ~ δDISOGSM2 + storms
Fixed effects		
Analysis of variance(F-test)		
Intercept	390.51/ 0.0001***	315.61/ 0.0001***
δDISOGSM2	296.80/ 0.0001***	264.28/ 0.0001***
typhoon	26.28/ 0.0001***	/
storms	/	20.12/ 0.0001***
Coefficients table (coefficient/ SE/p-value)		
Intercept	42.62/ 3.73/ p=0	41.67/ 3.87/ p=0
δDISOGSM2	0.45/ 0.03/ p=0	0.44/ 0.03/ p=0
typhoon	-25.31/ 4.94/ p=0	/
storms	/	-18.55/ 4.14/ p=0
Variance Function (95% CI)	expon -0.013 (-0.018, -0.007)	expon -0.015 (-0.021, -0.0096)
Correlation Structure (95% CI)	corCAR1(form = ~ time | site) 0.21 (0.11, 0.37)	corCAR1(form = ~ time | site) 0.25 (0.14, 0.40)
Scale (σ)	8.14 (6.97, 9.50)	7.90 (6.76, 9.24)

Table S3. Summary of best fitted GLS models for the relationship between the GNIP sites' precipitation δD and isoGSM2 δD values [13,18] with typhoon/ heavy storms as mixed effects. Prec = monthly precipitation amount (mm), δD_{precip} = δD values of the modern precipitation.

253 **References**

254 1. Croudace, I. W., Rindby, A. & Guy Rothwell, R. ITRAX: description and evaluation of a
255 new multi-function X-ray core scanner. *Geological Society, London, Special Publications*
256 vol. 267 51–63 (2006).
257 2. E. Abada Gatumbato, W. Carandang, N. Pampolina, N. A. Mallar, S. Narvadez. *Final*
258 *Report: Physical and Geopolitical Characteristics, Biological Resources, Socio-Cultural*
259 *and Economics Conditions and Institutional Arrangements/Governance of the Bulusan*
260 *Volcano Natural Park*. (2011).
261 3. Ruxton, G. D. The unequal variance t-test is an underused alternative to Student's t-test and
262 the Mann–Whitney U test. *Behavioral Ecology* vol. 17 688–690 (2006).
263 4. Yan, H. *et al.* Dynamics of the intertropical convergence zone over the western Pacific
264 during the Little Ice Age. *Nature Geoscience* vol. 8 315–320 (2015).
265 5. Feakins, S. J. *et al.* Production of leaf wax n-alkanes across a tropical forest elevation
266 transect. *Organic Geochemistry* vol. 100 89–100 (2016).
267 6. Maffei, M. Chemotaxonomic significance of leaf wax alkanes in the gramineae. *Biochemical*
268 *Systematics and Ecology* vol. 24 53–64 (1996).
269 7. Kershaw, A. P. & Strickland, K. M. A 10 year pollen trapping record from rainforest in
270 northeastern Queensland, Australia. *Review of Palaeobotany and Palynology* vol. 64 281–
271 288 (1990).
272 8. Bush, M. & Rivera, R. Pollen dispersal and representation in a neotropical rain forest. *Global*
273 *Ecology and Biogeography* vol. 7 379–392 (1998).
274 9. Rodionov, S. N. A sequential algorithm for testing climate regime shifts. *Geophysical*
275 *Research Letters* vol. 31 (2004).
276 10. Rodionov, S. N. Use of prewhitening in climate regime shift detection. *Geophysical*
277 *Research Letters* vol. 33 (2006).
278 11. R Core Team, R: A language and environment for statistical computing, 354.
279 <http://www.R-project.org/> (Foundation for Statistical Computing, Vienna, Austria, 355

2013).

12. Seddon, A. W. R., Froyd, C. A., Witkowski, A. & Willis, K. J. A quantitative framework for analysis of regime shifts in a Galápagos coastal lagoon. *Ecology* vol. 95 3046–3055 (2014).
13. IAEA/WMO, Global Network of Isotopes in Precipitation: The GNIP Database, 380. <http://www.iaea.org/water> (2017).
14. Pinheiro, J. C. & Bates, D. M. Mixed-Effects Models in Sand S-PLUS. *Statistics and Computing* (2000) doi:10.1007/978-1-4419-0318-1.
15. J. C. Pinheiro, D. M. Bates, S. DebRoy, D. Sarkar, R Core Team. *nlme: Linear and Nonlinear Mixed Effects Models, R package*. (2016).
16. Gałecki, A. & Burzykowski, T. *Linear Mixed-Effects Models Using R: A Step-by-Step Approach*. (Springer Science & Business Media, 2013).
17. Akaike, H. Information theory and an extension of the maximum likelihood principle. in *Second International Symposium on Information Theory* (ed. B. Petrov, F. C.) (Akadémiai Kiado, 1973).
18. Yoshimura, K. Stable Water Isotopes in Climatology, Meteorology, and Hydrology: A Review. *Journal of the Meteorological Society of Japan. Ser. II* vol. 93 513–533 (2015).
19. Wickham, H. *ggplot2: Elegant Graphics for Data Analysis*. (Springer Science & Business Media, 2009).
20. Bard, E., Raisbeck, G., Yiou, F. & Jouzel, J. Solar irradiance during the last 1200 years based on cosmogenic nuclides. *Tellus B: Chemical and Physical Meteorology* vol. 52 985–992 (2000).
21. Muscheler, R. *et al.* Reply to the comment by Bard et al. on 'Solar activity during the last 1000yr inferred from radionuclide records'. *Quaternary Science Reviews* vol. 26 2304–2308 (2007).
22. E. Bard, G. Raisbeck, F. Yiou, J. Jouzel. Reconstructed Solar Irradiance Data. *IGBP PAGES/World Data Center for Paleoclimatology, Data Contribution Series #2003-006 (NOAA/NGDC Paleoclimatology Program, Boulder CO, USA* (2003).

307 23. Juggins, S. *rioja: Analysis of Quaternary Science Data*. (2015).
308 24. Blaauw, M., Christen, J. A., Mauquoy, D., van der Plicht, J. & Bennett, K. D. Testing the
309 timing of radiocarbon-dated events between proxy archives. *The Holocene* vol. 17 283–288
310 (2007).
311 25. Blaauw, M. & Andrés Christen, J. Flexible paleoclimate age-depth models using an
312 autoregressive gamma process. *Bayesian Analysis* vol. 6 457–474 (2011).
313 26. M. Blaauw, J. A. Christen, Bacon, 352.
314 <http://www.chrono.qub.ac.uk/blaauw/bacon.html&gt. (2015).